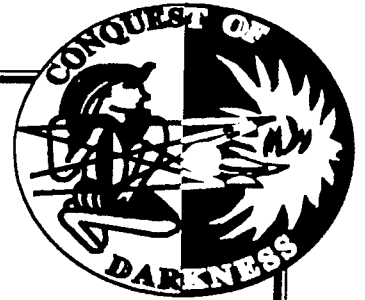


CECOM-TR-90-PO22-F



EFFICIENT TUNABLE VISIBLE LASER SOURCE

Dr. David C. Brown, Mr. David P. Benfey
Mr. Alec Robbins

Dr. Steven Davis, Dr William Kessler
Dr. Evan Pugh, M. G. Allen

Laser Technology Associates, Inc.
25 Ozalid Road
Johnson City, New York 13790

Physical Sciences, Inc.
20 New England Business Center
Andover, MA 01810

FINAL REPORT
November 1, 1992

**NIGHT VISION & ELECTRONIC SENSORS DIRECTORATE
(NVESD)
AMSEL-RD-NV-SE-EOIR
FORT MONMOUTH, NJ 07703-5206**

U. S. Army Contract # DAAB07-90-C-P022

Period of Contract: August 31, 1990 through December 4, 1992

**APPROVED FOR PUBLIC RELEASE;
DISTRIBUTION IS UNLIMITED.**

**COMMUNICATIONS - ELECTRONICS COMMAND (CECOM)
FORT MONMOUTH, NJ 07703-5206**

19950227 152

REPORT DOCUMENTATION PAGE

Form Approved
OMB No. 0704-0188

Public reporting burden for this collection of information is estimated to average 1 hour per response, including the time for reviewing instructions, searching existing data sources, gathering and maintaining the data needed, and completing and reviewing the collection of information. Send comments regarding this burden estimate or any other aspect of this collection of information, including suggestions for reducing this burden, to Washington Headquarters Services, Directorate for Information Operations and Reports, 1215 Jefferson Davis Highway, Suite 1204, Arlington, VA 22202-4302, and to the Office of Management and Budget, Paperwork Reduction Project (0704-0188), Washington, DC 20503.

1. AGENCY USE ONLY (Leave blank)		2. REPORT DATE November 1, 1992	3. REPORT TYPE AND DATES COVERED Final Report: 31 Aug 90 to 4 Dec 92	
4. TITLE AND SUBTITLE EFFICIENT TUNABLE VISIBLE LASER SOURCE			5. FUNDING NUMBERS C: DAAB07-90-C-P022	
6. AUTHOR(S) David Brown, David Benfey, Steven Davis, William Kessler, et al.				
7. PERFORMING ORGANIZATION NAME(S) AND ADDRESS(ES) * (Principal contractor:) Laser Technology Associates, Inc. 25 Ozalid Road Johnson City, NY 13790 (*also, see Block 11)			8. PERFORMING ORGANIZATION REPORT NUMBER	
9. SPONSORING/MONITORING AGENCY NAME(S) AND ADDRESS(ES) US Army Communications-Electronics Command (CECOM) Night Vision & Electronic Sensors Directorate ATTN: AMSEL-RD-NV-SE-EOIR (C. Pearce) Fort Monmouth, NJ 07703-5206			10. SPONSORING/MONITORING AGENCY REPORT NUMBER CECOM-TR-90-P022-F	
11. SUPPLEMENTARY NOTES This is an SBIR Phase II report. (*Sub-contractor: Physical Sciences, Inc., 20 New England Business Center, Andover, MA 01810)				
12a. DISTRIBUTION/AVAILABILITY STATEMENT Approved for public release; distribution is unlimited.			12b. DISTRIBUTION CODE DTIC ELECTE MAR 03 1995 S G D	
13. ABSTRACT (Maximum 200 words) In this final report, we summarize the design and performance of an optically phase-conjugated tunable visible dye laser system, and the frequency doubled Q-switched Nd:YAG laser used to drive it. This high-brightness laser source utilized optical phase-conjugation (OPC) via Stimulated Brillouin Scattering (SBS) in a double-passed dye laser cell containing Rhodamine 6G in methanol. The dye cell itself served as the SBS active medium. The use of SBS to remove optical aberrations in laser systems is relatively well-known; the implementation described herein is unique and can be used to provide a very compact tunable laser source. We have produced a 56% improvement in beam brightness and a 2.74 times improvement in beam jitter using the SBS in the double passed amplifier over using an ordinary retro mirror. This increase in beam brightness is due to a significant improvement in beam quality, and some pulse compression, obtained by using SBS. Output energy/pulse of 23 mJ has been demonstrated at 10 Hz and 560 nm output wavelength; tunability from 554 to 574 nm has also been demonstrated. DTIC QUALITY INSPECTED 4				
14. SUBJECT TERMS Dye lasers; optical phase conjugation; tunable lasers; visible lasers; Stimulated Brillouin Scattering; SBS; beam brightness; beam jitter			15. NUMBER OF PAGES 42	
			16. PRICE CODE	
17. SECURITY CLASSIFICATION OF REPORT Unclassified	18. SECURITY CLASSIFICATION OF THIS PAGE Unclassified	19. SECURITY CLASSIFICATION OF ABSTRACT Unclassified	20. LIMITATION OF ABSTRACT UL	



Laser Technology Associates, Inc.

25 Ozalid Road • Johnson City • N.Y. • 13790 • (607) 798-9064 • FAX (607) 798-9911

Efficient Tunable Visible Laser Source

November 1, 1992

U.S. Army Small Business Innovation Research
Phase II Contract # DAAB07-90-C-P022

FINAL REPORT

Period of Contract: August 31, 1990 Through December 4, 1992

Prepared For:

U.S. Army CECOM, EW/RSTA Center
AMSEL-RW-EW-S
Fort Monmouth, New Jersey 07703-5000
Attn: Dr. Carol Pearce

Prepared By:

Laser Technology Associates, Inc.
25 Ozalid Road
Johnson City, New York 13790

Physical Sciences, Inc.
20 New England Business Center
Andover, MA 01810

<input checked="" type="checkbox"/>
<input type="checkbox"/>
<input type="checkbox"/>

Project Contributors:

Dr. David C. Brown, Principal Investigator
Mr. David P. Benfey, Mr. Alec Robbins
Mr. Ken Smith, Mr. Joseph Watkins
Mr. Mark Scolpino, Mr. Richard Boyd
Ms. LaVaun Tanzini

Dr. Steven Davis, Dr. William Kessler
Dr. Evan Pugh, M.G. Allen

ty Codes

Dist	Avail and/or Special
A-1	

For a period of two (2) years after delivery and acceptance of the last deliverable item under the above contract, this technical data shall be subject to the restrictions contained in the definition of "Limited Rights" in DFARS clause at 252.227-7013. After the two-year period, the data shall be subject to the restrictions contained in the definition of "Government Purpose License Rights" in DFARS clause at 252.227-7013. The Government assumes no liability for unauthorized use or disclosure by others. This legend, together with the indications of the portions of the data which are subject to such limitations, shall be included on any reproduction hereof which contains any portions subject to such limitations and shall be honored only as long as the data continues to meet the definition on Government purpose license rights.

The views, opinions, and/or findings contained in this report are those of the author(s) and should not be construed as an Official Department of the Army position, policy, or decision, unless designated by other documentation. The contractor, Laser Technology Associates, Inc., certifies that, to the best of its knowledge and belief, the technical data delivered herewith under Contract Number DAAB07-90-C-P022 is complete, accurate, and complies with all requirements of the contract.

12/4/92

Date

Dr. David C. Brown, Principal Investigator

I. Executive Summary

In this Final Report we summarize the design and performance of an optically phase-conjugated tunable visible dye laser system, and the frequency doubled Q-switched Nd:YAG laser used to drive it. This high-brightness laser source utilized optical phase-conjugation (OPC) via Stimulated Brillouin Scattering (SBS) in a double-passed dye laser cell containing Rhodamine 6G in methanol. The dye cell itself served as the SBS active medium. The use of SBS to remove optical aberrations in laser systems is relatively well-known; the implementation described in this Final Report is unique and can be used to provide a very compact tunable laser source.

We have produced a 56% improvement in beam brightness and a 2.74 times improvement in beam jitter using the SBS in the double passed amplifier over using an ordinary retro mirror. This increase in beam brightness is due to a significant improvement in beam quality, and some pulse compression, obtained by using SBS.

Output energy/pulse of 23 mJ has been demonstrated at 10 Hz and 560 nm output wavelength; tunability from 554 to 574 nm has also been demonstrated.

Phase-conjugated output was obtained at a repetition rate up to 18 Hz, limited only by the laser power supply. No change in the output of the phase-conjugated dye laser occurred over a six month period (10^5 laser shots), indicating that little or no dye degradation occurred from the 532 nm pump nor the SBS process.

Our experiments, described in detail in this Final Report, indicate that compact tunable high brightness visible lasers can become a reality in the near term. Our proof-of-principle demonstration system utilized a modified commercial dye laser system which was not optimized for efficiency nor compactness. The availability of high-brightness tunable visible lasers will lead to advancements in the state-of-the-art of military countermeasure lasers and commercial scientific lasers.

Work described in this Final Report was performed at Laser Technology Associates, Inc. (LTA) facilities in Johnson City, NY, and at the facilities of LTA's subcontractor, Physical Sciences, Inc. (PSI), in Andover, MA.

II. Introduction

This document is the Final Report for U.S. Army Phase II Small Business Innovation Research (SBIR) Contract #DAAB07-90-C-P022, entitled "Efficient Tunable Visible Laser Source." The primary goal of this contract was to demonstrate the feasibility of using OPC via SBS to improve the beam-quality of tunable visible dye lasers. A second goal was to experimentally implement the concept previously generated during a companion Phase I SBIR contract (# DAAB07-88-C-P035) in which the final double passed dye laser amplifier was also used to provide the SBS medium (i.e. the dye dissolved in methanol). We have successfully achieved both of these goals.

Tunable visible dye lasers have a myriad of applications that can generally be categorized as military or commercial. Commercial applications are the most well-known and include medical, scientific, remote sensing, etc. The laser described in this Final Report appears to have several advantages when compared to present commercially available dye lasers. Due to a significant increase in beam brightness, the laser will make an ideal source for nonlinear experiments. For example, frequency doubling or tripling should be more efficient. In addition, we have found that the output beam angular jitter is significantly

improved. While not investigated during this program, we also expect a significant decrease in the amount of amplified spontaneous emission (ASE) present in the output beam due to the nature of the SBS process.

Military applications primarily involve the use of tunable dye lasers in countermeasure systems. Tunability is a desirable feature in modern military systems since laser output is more difficult to detect. It is desirable that a military system be able to produce a desired intensity on a target at range; optical aberrations in the laser system and in the atmosphere however reduce the obtainable intensity. By eliminating the optical aberrations inherent in the laser system itself, by using OPC, a significant increase in on target intensity can be obtained. Another important point is that the same intensity on target can be achieved with less dye laser output (e.g. a smaller laser). As described in detail below, during this program we have demonstrated that OPC in the dye medium itself appears to be a practical and reliable way of achieving a major improvement in the beam quality and brightness of conventional military and commercial dye laser systems.

In this Final Report, we describe in Section III the design and development of the Nd:YAG source operating at 1064 nm. In Section IV we show our frequency doubling results, resulting in a green 532 nm beam that makes a near ideal pump for the tun-

able dye laser source. Section V details the tunable dye laser experiments. Finally, in Section VI, we summarize the results obtained under this contract and make recommendations for further development (referred to as Phase III in the SBIR program).

III. Nd:YAG Laser Design and Performance

Overall Design:

We chose to design and demonstrate a frequency doubled pulsed Nd:YAG laser for use as a pump source for the tunable dye laser system. The original concept is shown in Figure 1; an oscillator/amplifier system was envisioned where the output of a single longitudinal mode (SLM) oscillator was double passed through a following Nd:YAG amplifier. Double passing was provided by Stimulated Brillouin Scattering (SBS) in a high-pressure cell. The resulting phase conjugation would remove thermally induced aberrations in the amplifier cell, leading to a near diffraction-limited output ideal for frequency doubling. In order to achieve this with good efficiency, the oscillator was to be injection-locked using a diode-pumped Nd:YAG single frequency laser. The oscillator consisted of a pump chamber housing, a polarizer and Q-switch, a high reflector, and a variable reflectivity mirror (VRM) as an output coupler. A positive branch VRM resonator was

chosen to provide a smooth transverse output, good extraction efficiency, and good beam quality.

During the design phase of this laser it became apparent that a far more efficient and compact laser could be achieved by eliminating the amplifier stage in Figure 1 and increasing the oscillator rod diameter. Accordingly, we arrived at the final design shown in Figure 2 which is identical to the oscillator section of Figure 1 but with a larger rod diameter.

Pump Chamber Design and Characterization:

The pump chamber design chosen is shown in an end-on view in Figure 3. Its construction consists of a *racetrack* fused silica solid body into which cooling channels were provided for the Nd:YAG rod and two Xe flashlamps. A silver coating was applied to the outside of the fused silica body. This highly efficient pump chamber design was arrived at by using an LTA developed pump chamber design code,

Figure 1. Original Q-Switched Nd:YAG System Concept

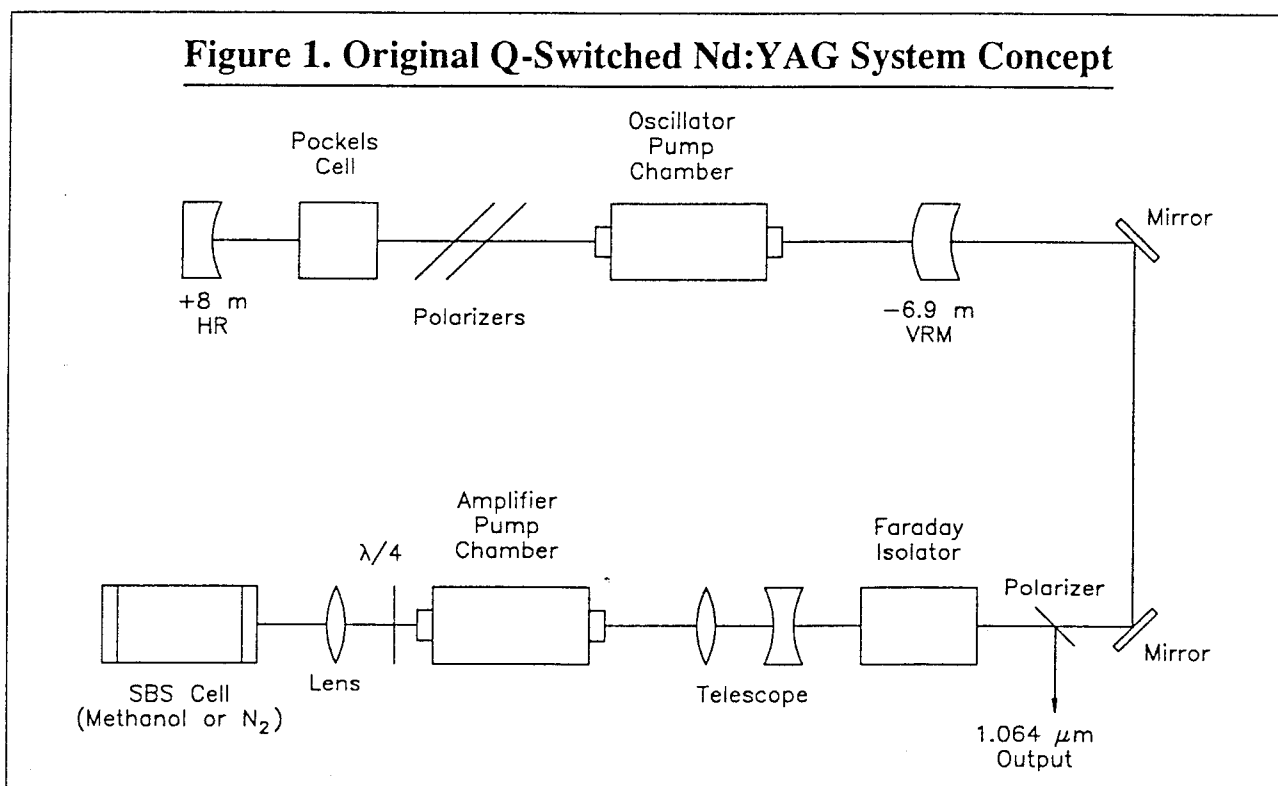
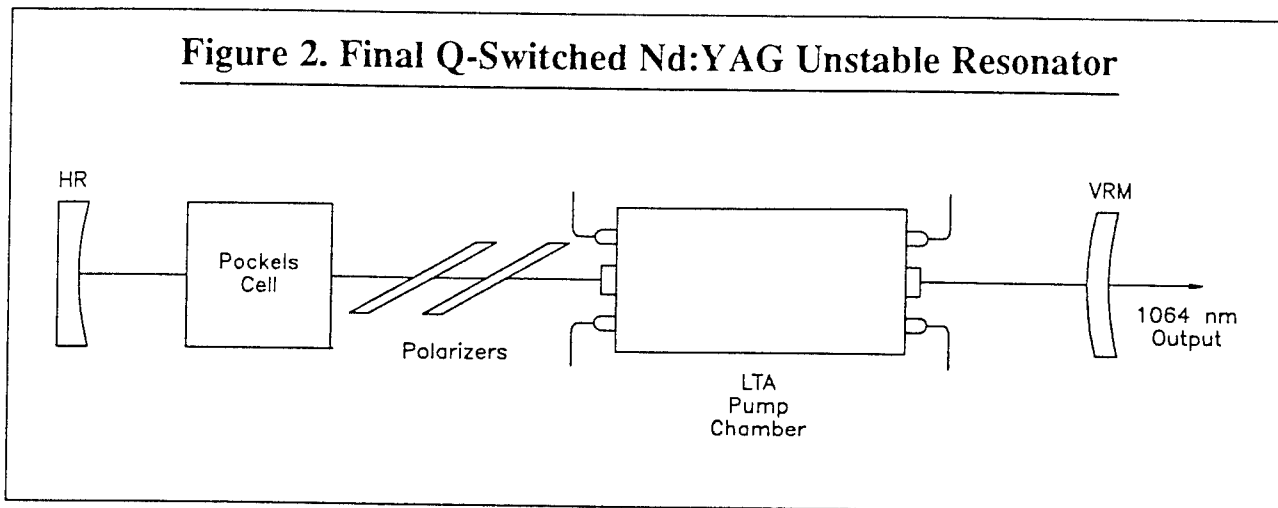


Figure 2. Final Q-Switched Nd:YAG Unstable Resonator



RAYOP [1,2]. RAYOP uses as its input empirically derived flashlamp spectral data generated with LTA's Spectral Characterization Facility (SCF). A measured flashlamp spectrum is shown in Figure 4. The Xe flashlamps, two of which were operated in series, had an 8 mm inside diameter, a 7.62 cm arc length, a 450 t fill pressure, and Cerium doped 1 mm thick fused silica walls. Two, rather than a single, lamps were chosen in order to provide a high degree of pumping symmetry in the Nd:YAG rod, thus eliminating any potential problems with non-uniform gain and heat deposition. The PFN provided a 250 μ sec pulsewidth (1/3 of maximum current), and up to 136 J/pulse stored.

In order to characterize the energy actually dissipated by the Xe flashlamps, we measured the lamp current and differential voltage to determine the transfer efficiency from PFN stored energy to energy dissipated by the lamp. The results are shown in

Figure 5 where the electrical transfer efficiency is plotted as a function of PFN stored energy. The resulting efficiency is approximately 71.6%.

Various shapes were considered for the pump chamber reflecting surface, including single and dual elliptical, close-coupled circular, racetrack, etc., and various combinations of these. An important consideration, however, was that the final pump chamber design be manufacturable and cost-effective. A number of considerations, including absorption efficiency and optical damage led us to choose a 9.5 mm diameter Nd:YAG rod. By using RAYOP we arrived at the racetrack design that provides excellent pumping uniformity and efficiency while satisfying our manufacturability and cost-effectiveness criteria. A 3-D profile of the predicted inversion uniformity is shown in Figure 6. At the design point of 102 J stored in the PFN, we determined that the transfer efficiency from the Xe flashlamps to upper level

Figure 3. Nd:YAG Laser Pump Chamber End View

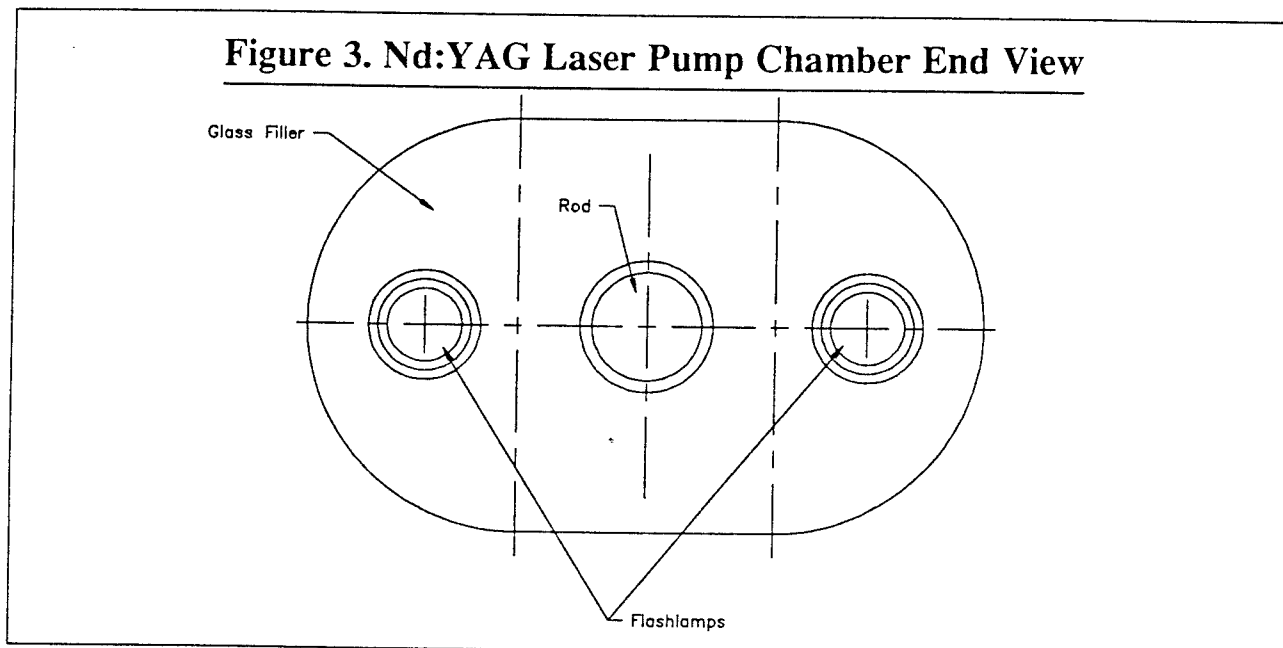


Figure 4. Nd:YAG Laser Flashlamp Spectrum

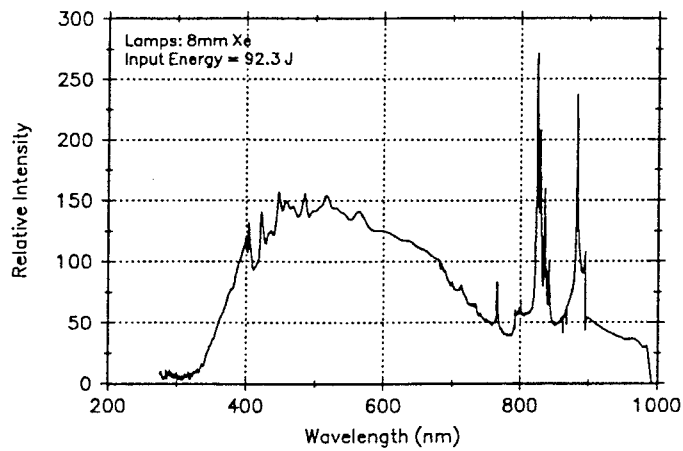


Figure 5. Lamp Energy vs. PFN Energy

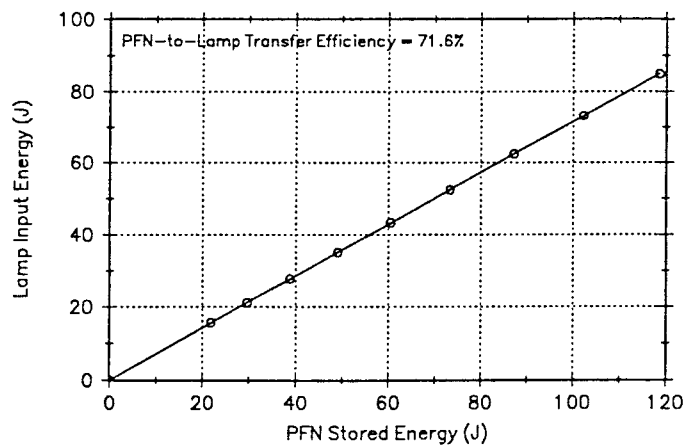
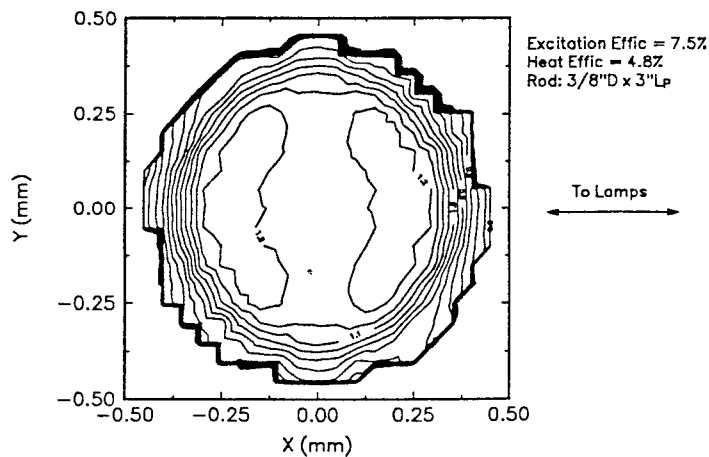


Figure 6. Nd:YAG Rod Excitation Profile



inversion using the racetrack configuration was 7.5%. The heat transfer efficiency was 4.8%.

We have also modeled the expected CW distortion and focal lengths of the Nd:YAG rod at various repetition rates (average power). In order to achieve this we used a finite element model to determine the radial (r), tangential (θ), and longitudinal (z) components of the thermally induced stress tensor. Contour plots of the three stress tensors for the Nd:YAG rod are shown in Figures 7-9 for a maximum expected heat power density of 25 W/cm^3 . In Figure 10 we show the expected optical path length difference (variation from the center), ΔOPL , for a flat-topped (phase) beam propagating through the rod, as a function of the rod radius and for the same heat loading. Shown are the various contributing effects, including change in index with temperature, index changes due to stress-induced birefringence, and rod end effects.

Using this model, we predicted the rod focal power as a function of rod average heat load for both the r - and θ -polarization components. This is shown in Figure 11 (the average is also shown). Also in Figure 11 we have plotted the rod focal length or power (average) determined experimentally by using a collimated HeNe laser and varying the average power delivered to the pump chamber. To get good agreement between theoretical and experimental data, a less than unity quantum efficiency of 0.70-0.75 was assumed, thus increasing the heat load.

Following fabrication of the pump chamber and assembly, we first characterized the unit's small-signal gain. By using a stable CW Nd:YAG laser and photodiode with 1064 nm narrow bandpass filter, we determined the small-signal gain shown in Figure 12 as a function of lamp energy. It can be seen that the gain is nearly linear but begins to roll

Figure 7. Nd:YAG Rod Radial Stress Tensor

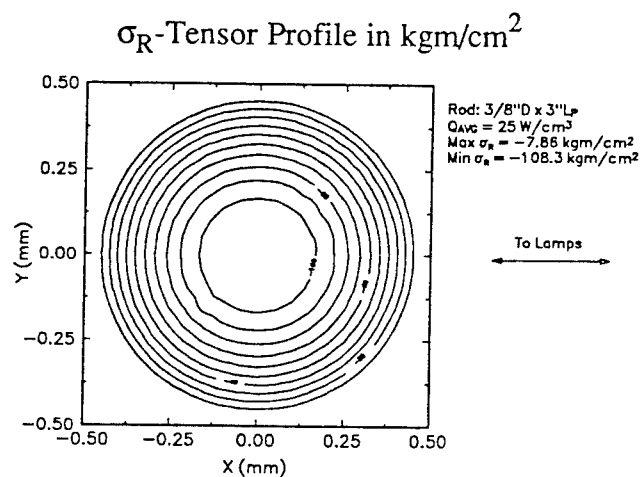


Figure 8. Nd:YAG Rod Tangential Stress Tensor

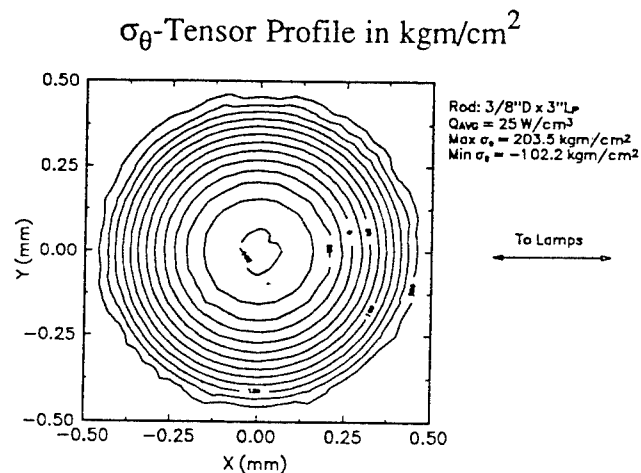


Figure 9. Nd:YAG Rod Longitudinal Stress Tensor

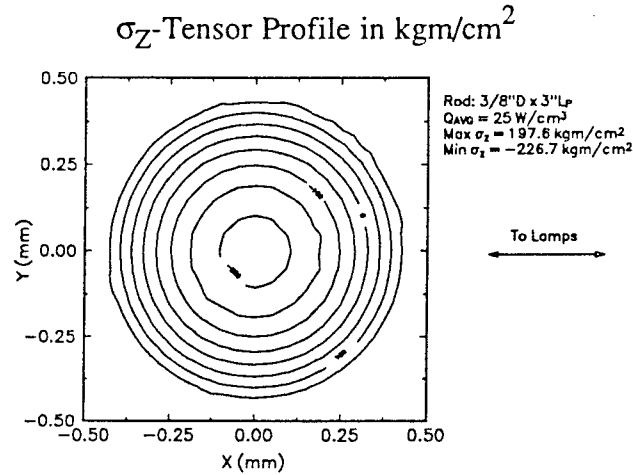


Figure 10. Nd:YAG Rod Optical Path Length Differences

Δ OPL Components and Total Radial and Tangential

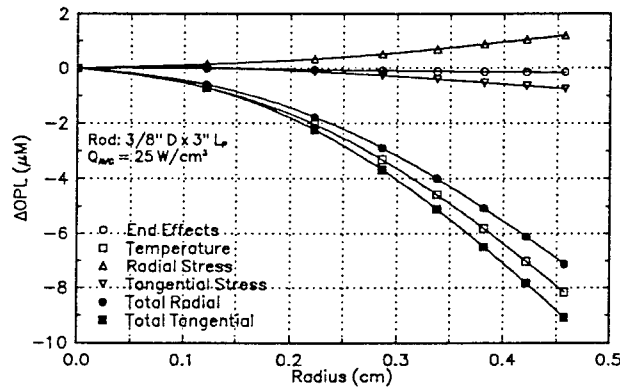
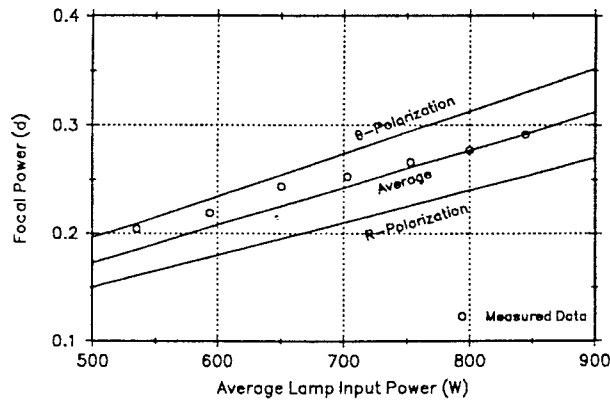


Figure 11. Nd:YAG Rod Focal Power vs. Input Power

Radial- and Tangential-Polarization Focal Power and Measured Data



off around a small-signal gain of 10. This rod has achieved a gain of 14, more than respectable for a 9.5 mm diameter rod. This high gain is attributed to the use of a coarser grit to roughen the rod barrel surface, making it more effective in suppressing the parasitics and amplified spontaneous emission (ASE) responsible for the roll off in gain in Figure 12. The small-signal gain is a direct measure of the amount of energy stored in the rod available for Q-switching. It can be seen from Figure 12 that approximately 1.9 J of extractable Q-switched energy is available at the peak lamp energy.

Following the gain characterization, we began extraction efficiency measurements to determine the pumping efficiency. A close-coupled hemispherical resonator was chosen for these experiments. In Figure 13 we show the configuration; a 2 m radius high reflector (HR), and a partial reflector (PR) out-coupler separated by 36 cm was used. In order to optimize the extraction efficiency, the value of the outcoupler reflectivity was varied. This resonator

configuration was chosen to insure that most energy was extracted from the entire rod volume. In Figure 14 we show the results of these experiments. The output energy is shown as a function of lamp input energy for outcoupler reflectivities of 40, 50, 60, 70, 80, and 90%. It can be seen that the optimum reflectivity is about 50%. An output energy/pulse of 2.5 J was achieved. Threshold was 9.0 J, and the slope efficiency was 3.28%. Following this data, we replaced the laser rod in the pump chamber and repeated the 50% outcoupler run. Shown in Figure 15, a slope efficiency of 3.65% was then demonstrated with an output of 2.8 J and a threshold of 8.4 J. The previous rod had shown a visible distortion around the barrel and was thus replaced.

If we use the maximum lamp energy shown in Figure 15, about 85 J, an estimated 50% radiative efficiency for the Xe flashlamps [3], and the calculated lamp-to-inversion transfer efficiency of 7.5%, almost 3.2 J of extractable energy was stored in the rod. We succeeded in extracting the majority of the

Figure 12. Nd:YAG Rod Small-Signal Gain vs. Lamp Input Energy

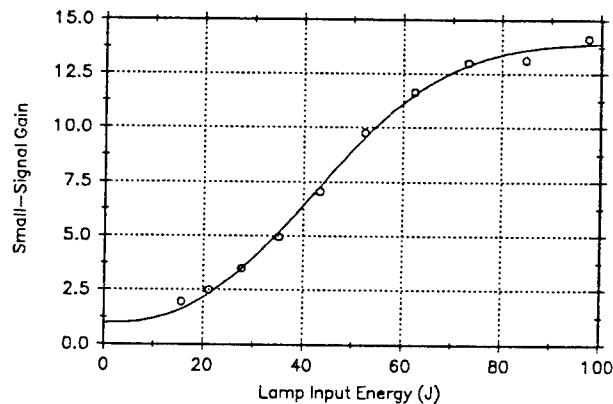


Figure 13. Nd:YAG Close-Coupled Hemispherical Resonator

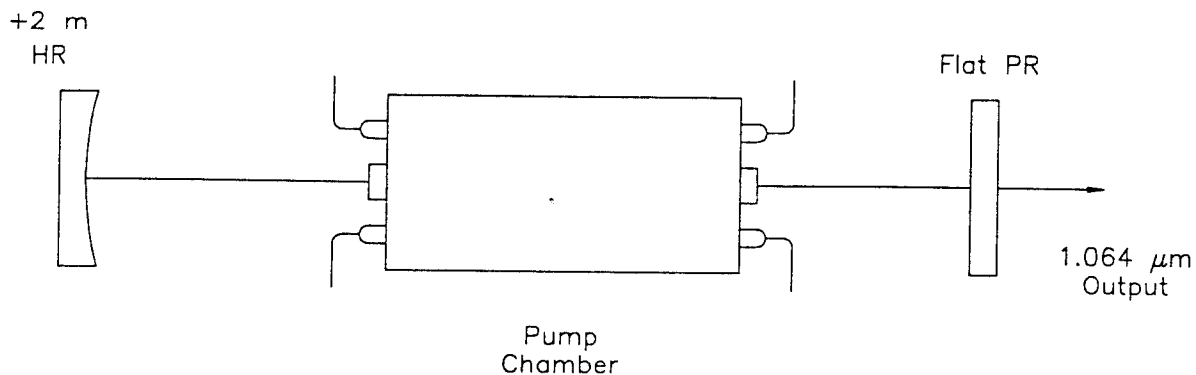


Figure 14. Nd:YAG Close-Coupled Hemispherical Resonator

Long Pulse Output vs. Input Energy

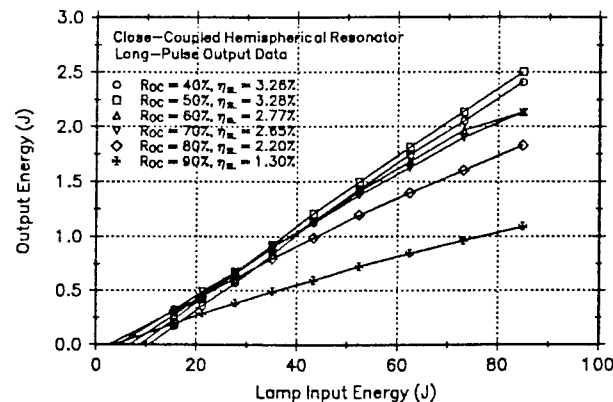
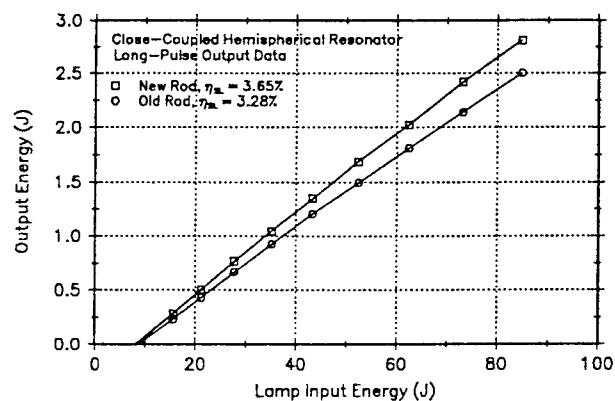


Figure 15. Nd:YAG Close-Coupled Hemispherical Resonator

Rerun of 50% Outcoupler with New Rod



stored energy in the long-pulse mode. The extraction efficiency was 85%, in agreement with our Rigrod extraction efficiency model. Note that the long-pulse energy is significantly higher than that predicted by the small signal gain in Figure 12 since once long-pulse extraction begins at threshold, parasitics, ASE, and fluorescence decay losses are minimal.

Following the close coupled long-pulse experiments described above, we switched to a longer hemispherical resonator and compared its long-pulse performance to the VRM unstable resonator with the same length. The hemispherical resonator used a +8 m HR and a flat 50% PR as an outcoupler. The magnification 1.15 VRM resonator used the same +8 m HR and a VRM outcoupler with a -6.9 m radius, an average reflectivity of 10%, a peak reflectivity of 15%, and a third-order super-Gaussian profile with a

waist of 2.4 mm. In Figure 16 we show the obtained long-pulse output energy as a function of flashlamp energy for both resonators. At a lamp energy of 85 J, the hemispherical and VRM resonators achieved 1.07 J and 1.05 J, respectively. The reduction in energy/pulse that occurs when compared to the close coupled hemispherical resonator of Figure 15 that achieved 2.8 J is due to the lower mode volume or rod fill of the longer resonators. The 70 cm long hemispherical resonator extracts only 39% of the available energy. The VRM resonator extracts only 38% although the average reflectivity is only 10%. On the other hand the VRM resonator extracts 98% of that achieved with the 70 cm long hemispherical resonator. These results indicate that, due to the reduced mode volume, about 720 mJ of stored energy is available for Q-switching.

Q-Switched Characterization:

Following our initial characterization of the pump chamber for long-pulse operation, we conducted a series of Q-switching experiments. We inserted a KD*P Pockels cell and two polarizers in the VRM resonator as previously shown in Figure 2. The measured extinction ratio of the polarizers was 400; two were used in order to suppress pre-lasing and parasitic modes expected due to the large round-trip gain of about 200. Measured transmission of the Pockels cell and the polarizers was greater than 99%. Pockels cell operation was in the quarter-wave ($\lambda/4$) mode. Measured $\lambda/4$ voltage was about 3250 V. Three separate Q-switch drivers were investigated, based on krytron, thyatron, and avalanche transistor switches. Pre- and post-pulse lasing were observed at the higher gains, depending upon the driver. The optimum driver found was the thyatron, with about a 15-20 nsec switching time and a 200 nsec recovery time. No detectable pre- nor post-lasing was observed with this driver, even at the highest gain level. A problem with all drivers was that the Pockels cell did not fully recover at the time the Q-switched pulse built up (typically 50 nsec at the highest gain). Typically, a 10-15% loss was encountered, reducing the Q-switched output and the laser efficiency. An improved driver would correct this, significantly increasing the output.

The laser was aligned for Q-switched operation by observing the output beam with an LTA developed video processing system (VPROC). The extinction voltage and Q-switch were adjusted to give complete extinction at the highest pumping energy. It was ensured that pre- and post-lasing were suppressed by monitoring with a fast photodiode and oscilloscope.

In Figure 17 we show the laser Q-switched output at a 1 and 10 Hz repetition rate. A maximum pulse

energy of 513 mJ was achieved at 1 Hz, and 378 mJ at 10 Hz. The optimum delay between flashlamp and Pockels cell firing was determined for each voltage (or lamp energy). Average power was thus 0.5 W at 1 Hz and 3.8 W at 10 Hz. The loss in efficiency as repetition rate is increased was due to the thermally induced birefringence in the rod, resulting in rejection at the polarizer. No techniques were implemented to reduce the average 26% birefringence loss. In Figure 18 we show the Q-switched pulsewidth for the 1064 nm (and 532 nm - to be discussed later) output as a function of lamp energy. It can be seen that a minimum pulsewidth of slightly less than 10 nsec was achieved for a lamp energy of 85 J; the resultant peak power was then 51.3 MW.

Analysis has shown that further significant increases can be achieved with this oscillator during Phase III. Of the approximately 1.88 J available for Q-switching, by comparison with the long-pulse results, we can access only 720 mJ with the VRM resonator. Our maximum output was 513 mJ or 71% of the available energy. Calculation has shown that with a more optimized Q-switch and driver, extraction efficiency can be increased to 85%, or 600 mJ. Further increases of up to 25% can be obtained by the incorporation of a Samarium (Sm) doped solid pump chamber body, optimization of the VRM reflectivity and profile, and further optimization of the Xe flashlamps. During the Phase III program we thus expect to achieve over 750 mJ of Q-switched energy/pulse. Further increases in efficiency and higher repetition rate performance can also be expected. We intend to implement a number of techniques for minimizing the effects of thermal focusing and birefringence, allowing efficient operation up to 50 Hz during Phase III.

VPROC was also used to obtain beam profiles from the laser. In Figure 19 we show output beam near-

Figure 16. Hemispherical and VRM Unstable Resonator

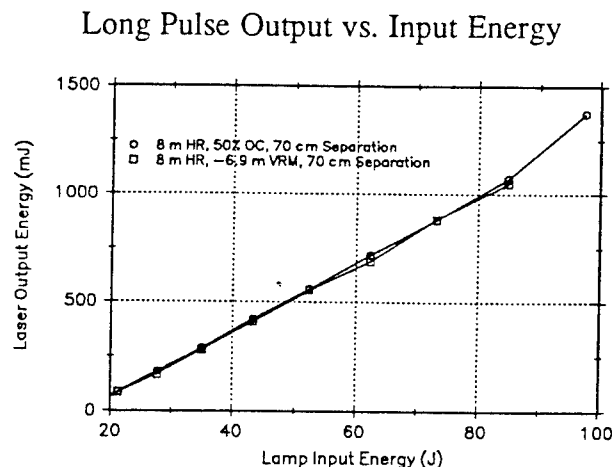
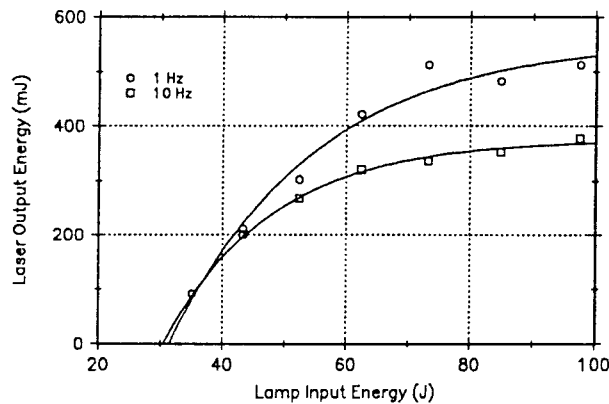
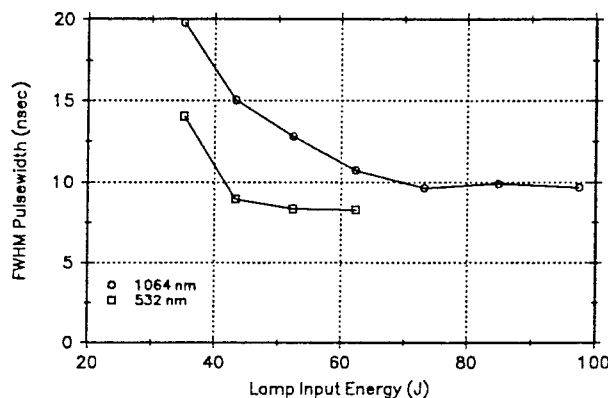


Figure 17. Q-Switched Output vs. Input Energy

VRM Unstable Resonator at 1 and 10 Hz Repetition Rate

**Figure 18. Q-Switched Pulsewidth vs. Lamp Energy**

VRM Unstable Resonator 1064 nm and (Doubled) 532 nm Pulsewidths



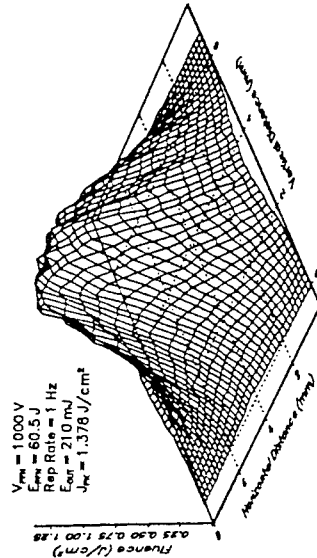
field profiles for three lamp energies, measured 150 cm from the VRM, and for a repetition rate of 1 Hz. In Figure 20 similar profiles are shown for 10 Hz. The slightly diamond shaped output profile in Figure 20 is characteristic of a laser operating with a thermally induced birefringence loss. Far-field beam profiles were also obtained with VPROC, using a 25 cm focusing lens. The near and far-field results were then used to obtain the beam quality. At 1 Hz the beam quality was 2.6 mm-mrad (diffraction-limited) for low lamp energy while at 85 J/pulse it deteriorated to 8.5 mm-mrad, or about 3.3 times, diffraction-limited. The change in beam quality with lamp energy is a consequence of the radially varying

gain and beam sizes with pump energy. The average beam quality for the resonator at 1 Hz was 6.5 mm-mrad or 2.5 times diffraction-limited. At 10 Hz, the beam quality varies between 8.5 mm-mrad at low lamp energy to almost 20 mm-mrad at 85 J/pulse. The primary reason for this is that the resonator was near-optimum only at 1 Hz. To achieve excellent beam quality at 10 Hz the power of the HR must be reduced to compensate for the rod focusing. This optimization was not attempted during this program due to programmatic constraints. In spite of the degraded beam quality at 10 Hz, as we show below we were still able to obtain acceptable second harmonic generation (SHG) efficiencies.

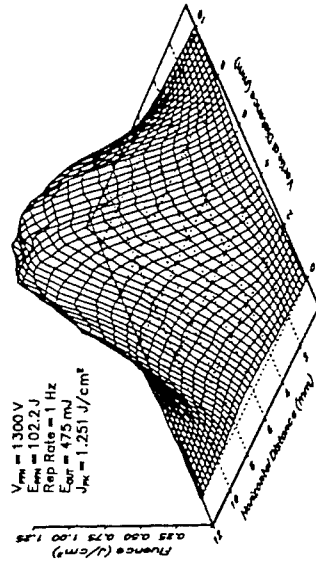
Figure 19. Nd:YAG Q-Switched Laser Near-Field Profiles

Various Pulse Energies at 1 Hz Repetition Rate

Lamp Energy = 43.3 J



Lamp Energy = 73.2 J



Lamp Energy = 97.4 J

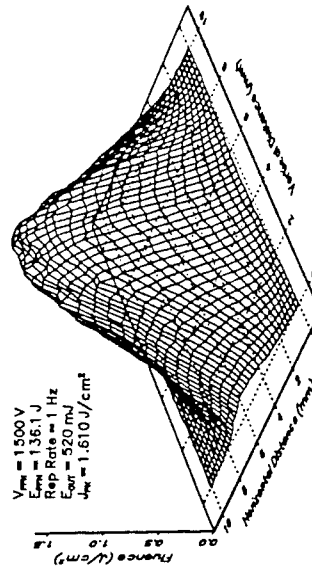
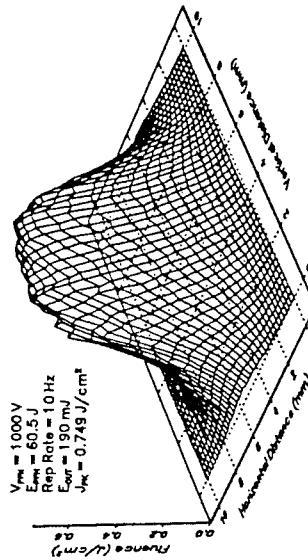


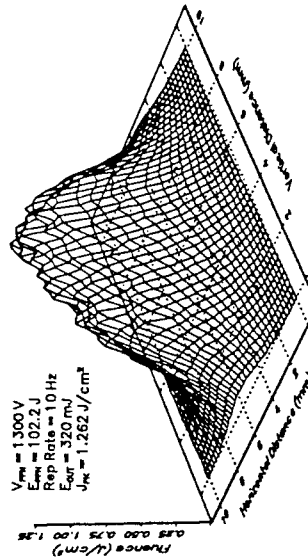
Figure 20. Nd:YAG Q-Switched Laser Near-Field Profiles

Various Pulse Energies at 10 Hz Repetition Rate

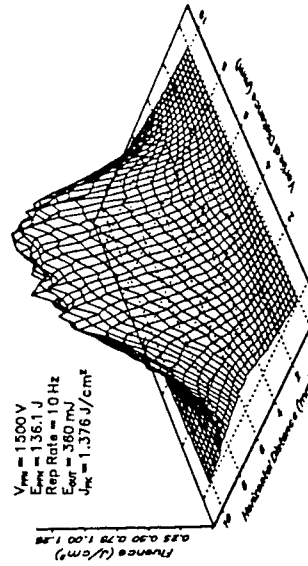
Lamp Energy = 43.3 J



Lamp Energy = 73.2 J



Lamp Energy = 97.4 J



IV. Second Harmonic Generation

In order to provide a pump-source for the tunable dye laser experiments, the 1064 nm Q-switched beam had to be converted to a visible wavelength. SHG was chosen to provide 532 nm output, near-ideal for pumping the Rhodamine 6G dye chosen for the dye laser. For good conversion and easy experimental implementation, we chose to use the nonlinear crystal KTP in a Type II phase-matching scheme. As shown in Figure 21, the 1064 nm beam is incident upon a half-wave ($\lambda/2$) waveplate that is used to select the polarization at an optimum angle of 45° with respect to the e- and o-axes of the crystal. The 532 nm light then emerges from the crystal with vertical polarization while the unconverted 1064 nm light emerges with horizontal polarization.

Following the SHG crystal, a 45° turning mirror was used to separate the 1064 nm and 532 nm light; the mirror was HR for 532 nm and maximally transmissive for 1064 nm.

For our initial experiments, a $6 \times 6 \times 7 \text{ mm}^3$ KTP crystal was used. Each face was anti-reflection (AR) coated for both wavelengths. A four axis mount was used to maximize conversion efficiency. In addition, a Galilean demagnifying telescope with a magnification of 1.3 was placed before the SHG crystal to reduce the beam size and provide collimation. The telescope lenses were AR coated at 1064 nm. With this setup we were able to achieve the conversion results shown in Figure 22 at a repetition rate of 1 and 10 Hz. Unfortunately, we damaged the output

Figure 21. Frequency Doubling Optical Layout

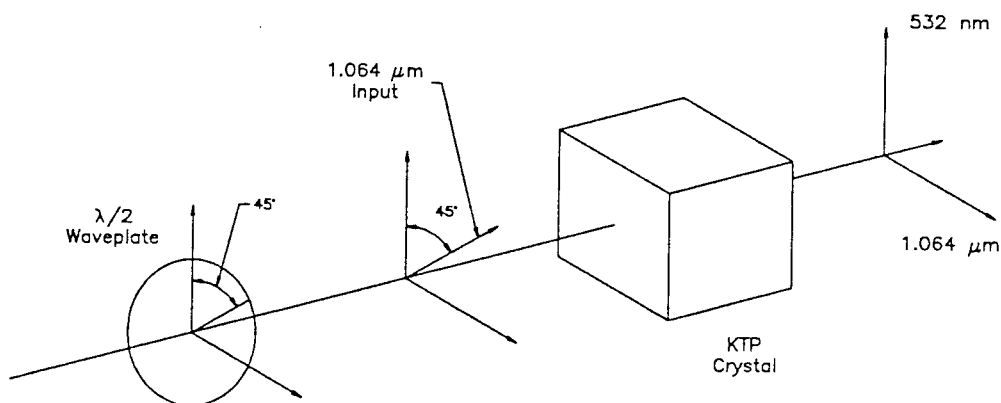
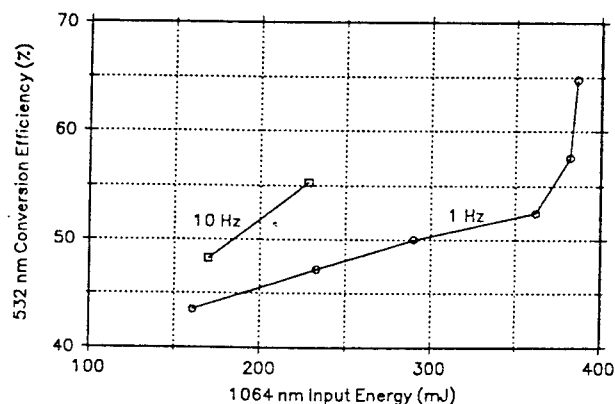


Figure 22. Frequency Doubling Conversion Efficiency

1 and 10 Hz Repetition Rate



face of the SHG crystal during these runs and were unable to finish the 10 Hz results. Nevertheless, we achieved a respectable 66% conversion efficiency. The significantly increased conversion efficiency at 1 Hz for the higher incident 1064 nm pulse energies is a consequence of the increase in peak power or intensity due to the increased energy/pulse and decreasing 1064 nm pulsewidth. The increased conversion at 10 Hz is due to a decreased spot size of the 1064 nm beam caused by rod thermal focusing.

Previously, in Figure 18, we showed the measured 1064 nm and 532 nm pulsewidths as lamp energy is varied. Note that the 532 nm beam has a shorter pulsewidth than the 1064 nm beam. This is a consequence of the nonlinear conversion process where the temporal pulse center converts efficiency whereas the wings have a much lower conversion efficiency. In Figures 23 and 24 we show near-field beam profile measurements of the 532 nm beam for

three different lamp pulse energies at 1 and 10 Hz, respectively. It can be seen that a smooth Gaussian-like radial profile is obtained at both repetition rates. Comparison of these beam profiles with the 1064 nm profiles indicates that the 532 nm beam is narrower than the 1064 nm, again because the beam spatial wings do not convert as efficiently as the more intense center.

Because of the KTP crystal damage, which made it unusable, we replaced it with a new AR coated 6x6x6 mm³ KTP crystal. In addition, we removed the Galilean telescope. Our 1064 nm output beam just fit in the 6x6 mm² aperture at 10 Hz, whereas at 1 Hz the crystal was overfilled at the higher pulse energies. Final demonstration of the system was achieved with the laser operating at 10 Hz and by limiting the crystal input energy to 160-170 mJ/pulse. Green output energy/pulse was then typically 80 mJ.

V. Dye Laser Performance

Stimulated Brillouin Scattering has important practical implications since the SBS process can be used to produce phase conjugated beams. Phase conjugation, first described by Zel'dovich [4] is applicable to a number of problems, for example, propagation through atmospheric turbulence, and beam clean-up through phase distorting gain media. Indeed, SBS has been used to improve the beam quality of stimulated radiation emanating from multipass amplifiers [5-7]. Recently, SBS produced in an intracavity gaseous SF₆ cell in a Nd:YAG laser was used to produce 100 mJ in a TEM₀₀ mode [8].

Tunable dye lasers, while offering many advantages such as tunable, high power output, often produce output beams that display poor beam quality. High power coaxial flashlamp systems are notorious for this behavior. Even more sophisticated dye systems, such as excimer and Nd:YAG laser pumped dye lasers, often suffer from this drawback. In laser pumped dye lasers, the dye oscillator and amplifier are often side pumped. This produces a non-uniform gain medium, transverse index of refraction gradient, and an associated high order transverse mode output beam.

The major goal of this program was to determine whether SBS could be used to produce a dye laser beam of enhanced beam quality. We also desired to demonstrate that the final power amplifier of a commercial dye laser could be used as the SBS cell in a compact configuration. Here we describe the results of our investigations.

Dye Laser Description:

The dye laser that we used as the testbed for this program was a Quantel model TDL 50. This commercial unit consists of an oscillator, preamplifier, and final amplifier. The oscillator design incorporates a grazing incidence grating and uses a Littrow mirror for wavelength tuning. Its linewidth is approximately 0.1 cm⁻¹. The preamplifier is a standard dye cuvette placed at Brewster's angle. The final amplifier is a unique capillary design which reduces amplified spontaneous emission effects and provides a more uniform gain medium. A block diagram of the dye laser is shown in Figure 25. This laser offered several advantages for the SBS tests. First, the oscillator restricts the laser to operate on only two or three longitudinal modes, making it easier to produce and verify SBS. Second, this laser was designed to be pumped by a Q-switched, frequency doubled Nd:YAG laser. Thus the optics were compatible with both a Quantel Nd:YAG pump source and the LTA Nd:YAG laser.

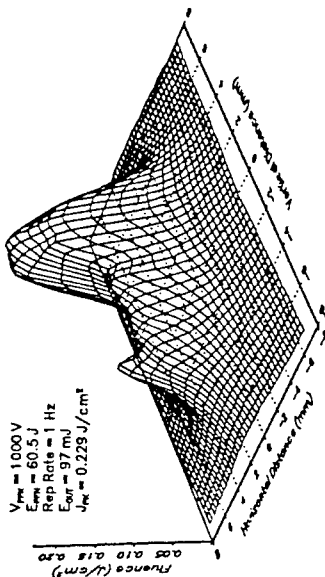
Our initial tests of the dye laser at PSI indicated that we could produce output pulse energies in excess of 50 mJ at a repetition rate of 10 Hz at 563 nm when pumped by our Quantel Nd:YAG laser system. We utilized methanol based Rhodamine 590 laser dye solutions as the gain media. The pulse length was approximately 10 nsec. At the completion of these initial tests, we began the SBS experiments.

The first Brillouin scattering studies were completed using the apparatus shown in Figure 26. The SBS cell was a rectangular dye cell (Lambda Physik

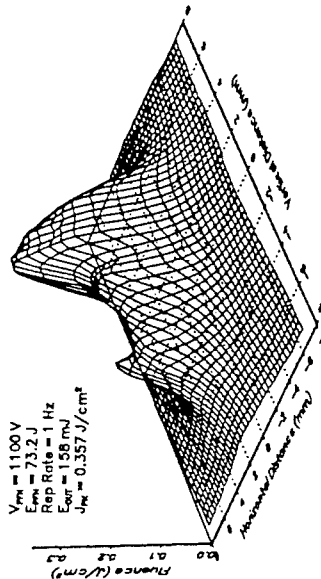
Figure 23. Nd:YAG Q-Switched Doubled (532 nm) Laser Near-Field Profiles

Various Pulse Energies at 1 Hz Repetition Rate

Lamp Energy = 43.3 J



Lamp Energy = 52.4 J



Lamp Energy = 62.3 J

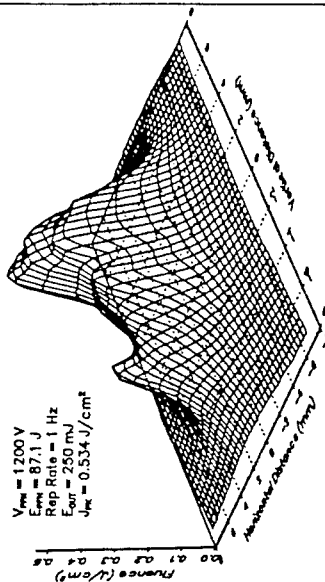
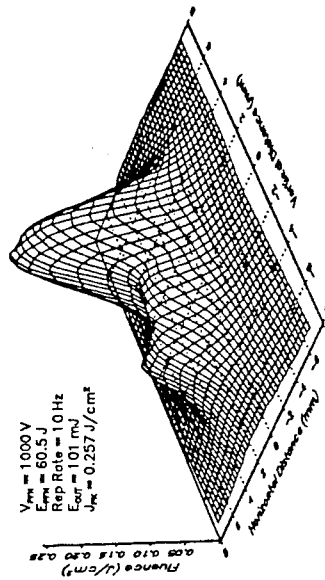


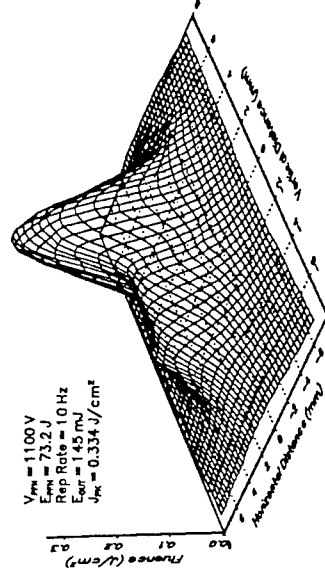
Figure 24. Nd:YAG Q-Switched Doubled (532 nm) Laser Near-Field Profiles

Various Pulse Energies at 10 Hz Repetition Rate

Lamp Energy = 43.3 J



Lamp Energy = 52.4 J



Lamp Energy = 62.3 J

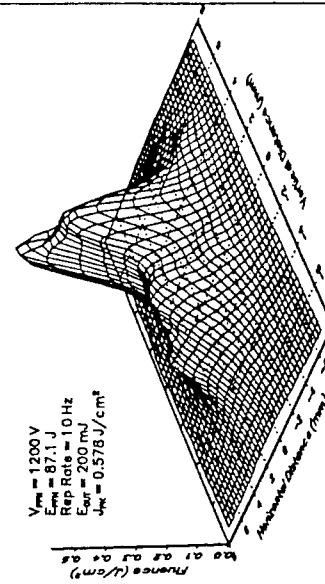
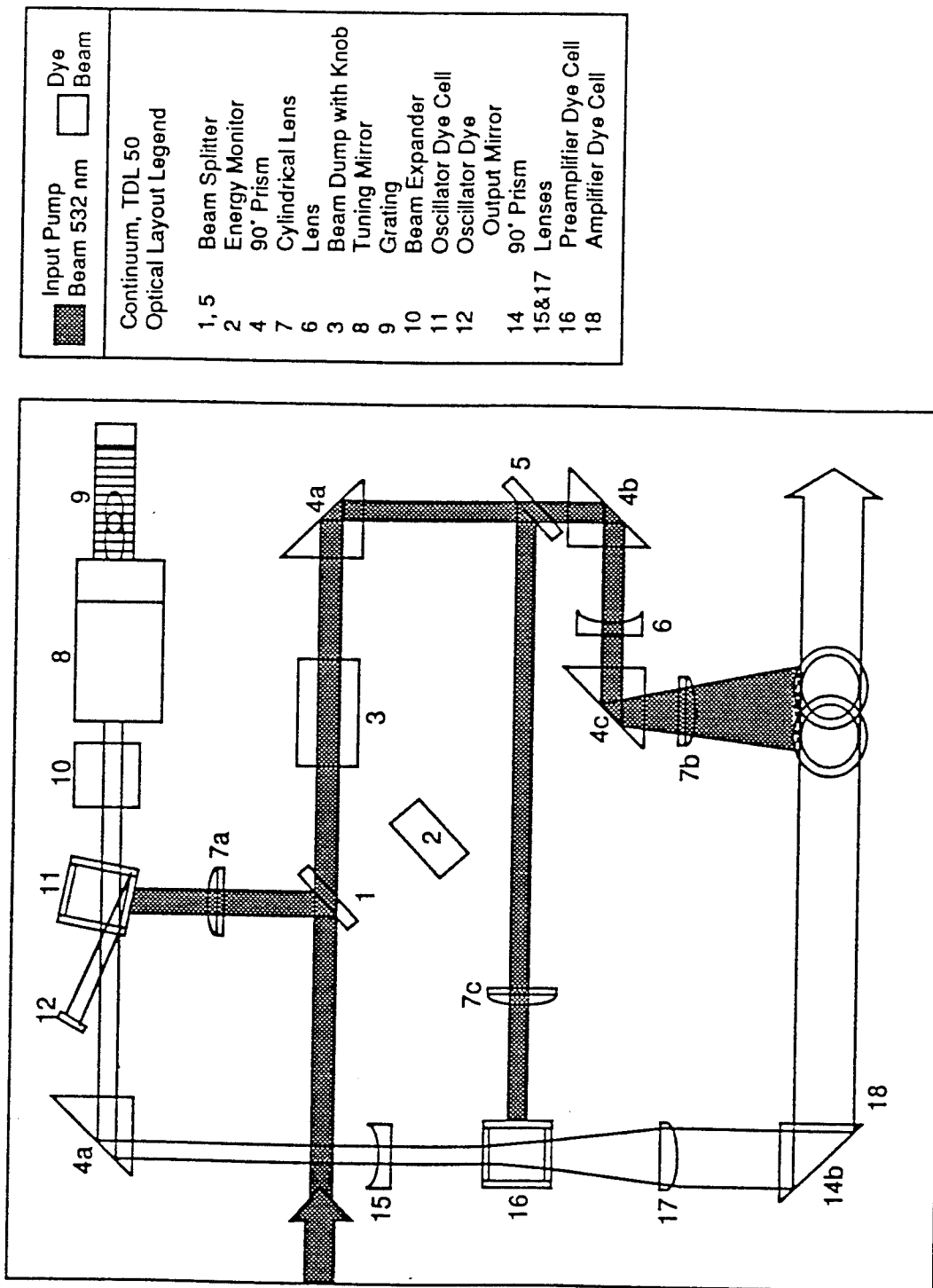
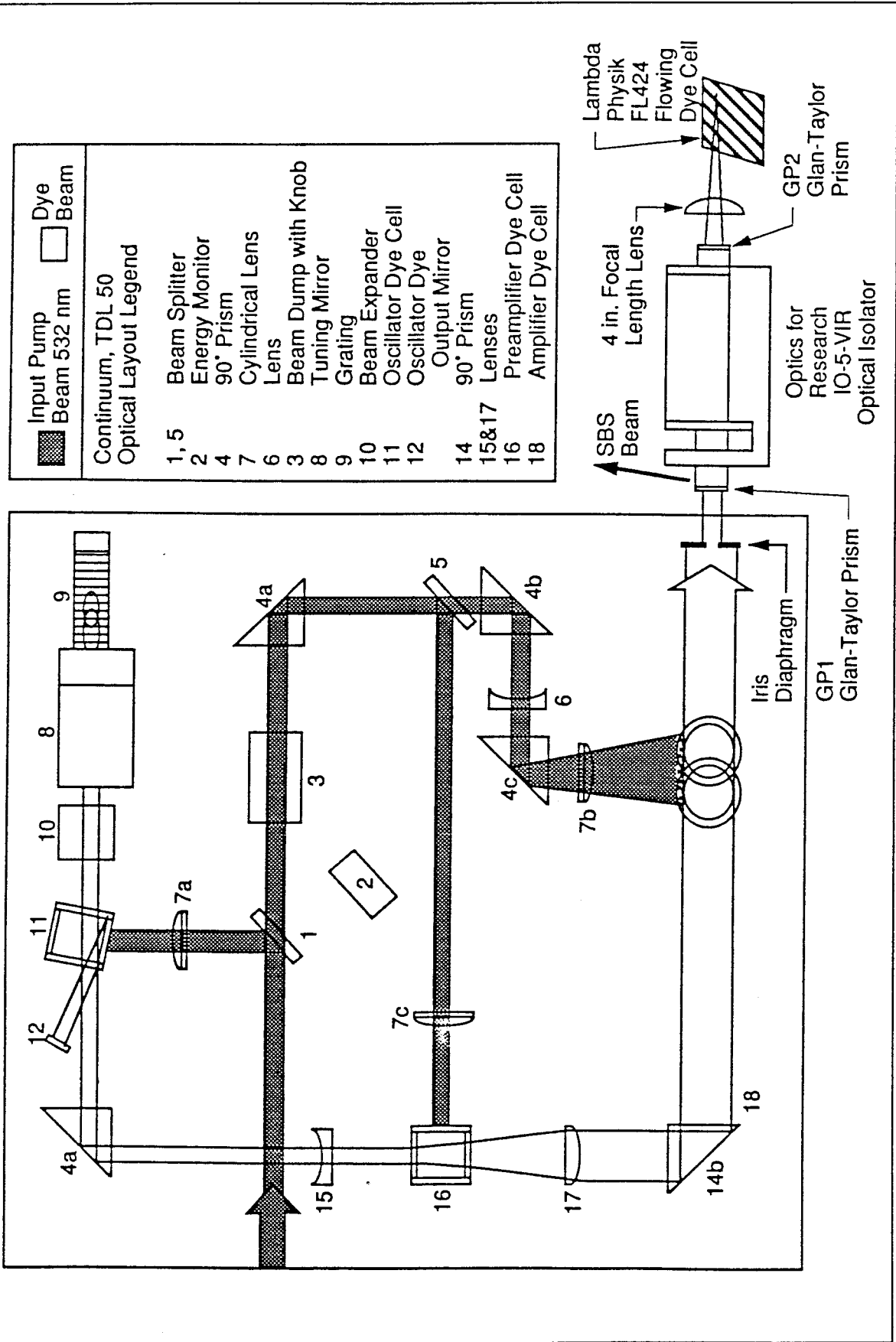


Figure 25. Block Diagram of Dye Laser Used for SBS Experiments



C-0364a

Figure 26. Dye Laser Setup for Initial SBS Demonstration



FL424) equipped with a flow circulation pump. The SBS mirror was created in this dye cell. We completed several series of tests using this configuration. A Faraday optical isolator (Optics for Research IO-5-VIR) was used to couple out the back propagating SBS beam. We note that prior to the arrival of the optical isolator from the vendor, we used optical flats at 45° to couple out some of the SBS beam. Our first observations of SBS were obtained using a 10 cm focal length lens to focus the dye beam into the methanol cell. The first indications of SBS were confirmed by the observation of a backward propagating beam that was precisely collinear with the initial dye beam. It propagated through every dye laser optical component shown in Figure 26 and was eventually diffracted off the grating of the dye oscillator. In these initial tests prior to the arrival of the Faraday rotator, we ran the SBS barely above threshold to avoid damage to the optical components in the dye oscillator. While this was not a satisfactory configuration for efficiency measurements, it was adequate for the spectroscopic measurements described below.

Spectroscopic Measurements:

In SBS the scattered wave is slightly red-shifted by the frequency of the acoustic wave that propagates through the liquid medium. The frequency shift, $\Delta\nu$, can be calculated from eqn. (1) [9].

$$\Delta\nu = 2 \nu_0 v n/c \quad (1)$$

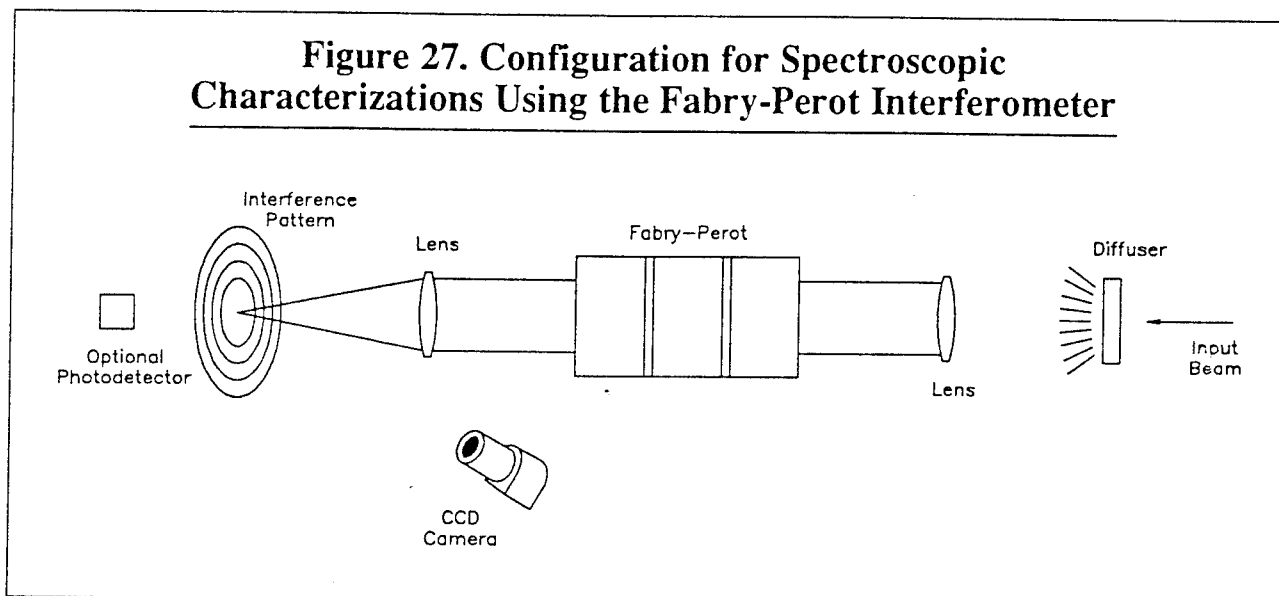
where ν_0 is the frequency of the incident light, v is the speed of sound in liquid (1.124 m/sec for methanol), n is the liquid index of refraction (1.326 for methanol), and c is the speed of light.

For methanol this frequency shift is approximately 0.176 cm^{-1} for excitation at 563 nm. Experimental observation of this frequency shift in the scattered beam with respect to the dye beam frequency was used to verify that the back-scattered beam was SBS.

The apparatus for these spectroscopic measurements is shown in Figure 27. We used a high resolution Fabry-Perot (F-P) interferometer to examine the spectral content of both the scattered beam and the dye beam. The F-P was a Burleigh model RC-140 with 5 cm diameter mirrors. In order to couple out the back-propagating SBS prior to the dye laser, we used optical flats placed at 45° with respect to the propagation direction of the laser beam. This permitted us to examine both the dye beam and the SBS beam. The output beams were passed through a diffuser plate and then collimated prior to entering the F-P. The diffuser plate removes the spatial coherence in the beam and transforms the beam into an extended source. The lens is used to collimate the light from this extended source. After transmission through the F-P the radiation is focused onto a flat screen. The focusing lens is used to form an image of the F-P interference pattern which consists of a series of concentric rings known as rings of equal inclination.

We examined the spectral content of an individual laser shot using a PSI designed CCD camera. We have designed and built several of these cameras for our flow diagnostics programs for NASP and for other applications. The camera incorporates a video format, and we can use a PC for data acquisition and subsequent analysis. The camera has several features that make it ideal for the present application. For example, it has a calibrated linear response and can be gated for periods of less than 1 μsec . The camera viewed the F-P pattern on the screen by gating the intensifier on during a laser pulse. We recorded the

Figure 27. Configuration for Spectroscopic Characterizations Using the Fabry-Perot Interferometer



spectra of individual pulses for both the dye and SBS outputs. Each image was digitized and stored for subsequent data analysis.

A typical digitized interferogram is shown in Figure 28. Pairs of rings are shown starting from the central spot of the interferogram. In Figure 29 we illustrate the analysis of the interferograms. A horizontal slice through the data in Figure 28 shows the intensity profile as a function of the pixel number. Several sets of doublets are shown each containing both the dye and SBS beam. The center of the interferogram corresponds to pixel number 350. The data displayed in Figure 29 are plotted in wavenumber space in Figure 30. In Figure 30 we have superimposed the data from the several rings shown in Figure 28. The diminishing resolution observed as we progress to

rings further from the center of the pattern is typically observed in F-P interferometers. We observed pairs of lines separated by 0.177 cm^{-1} , the shift expected for SBS scattering in methanol. These high resolution spectroscopic examinations confirmed that we were producing SBS radiation.

The F-P also allowed us to investigate the longitudinal mode structure of the dye laser beam. We usually observed one or two modes simultaneously lasing. An example of an interferometric spectrum showing three modes lasing is shown in Figure 31. The axial mode spacing was measured from the interferogram to be approximately 0.064 cm^{-1} . This is consistent with the cavity length of the dye laser oscillator.

Figure 28. Fabry-Perot Interferogram Obtained Using CCD Camera

Single Shot Images of Both the Dye Beam and the SBS Beam are Shown

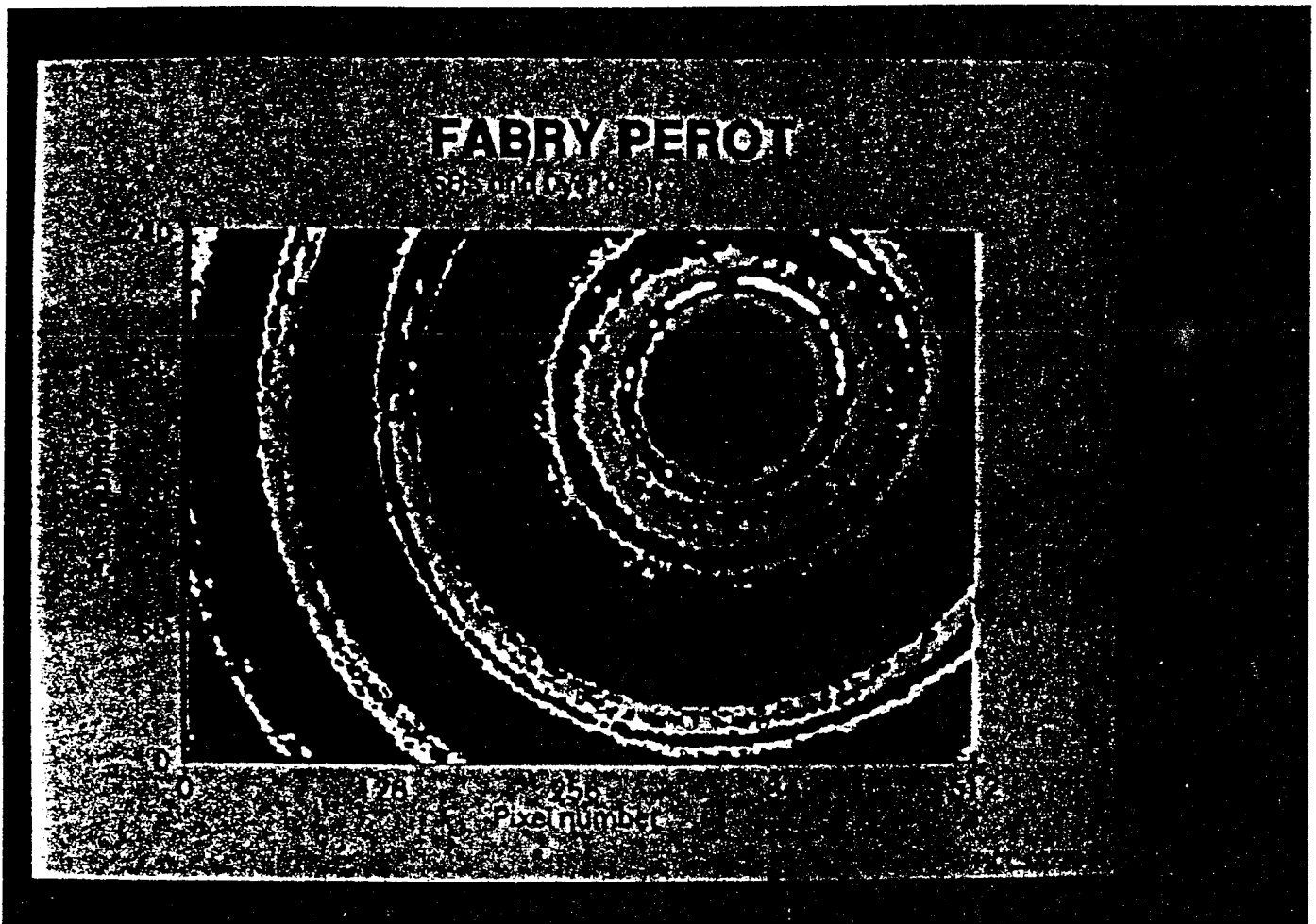


Figure 29. Data Displaying Slice Through the F-P Image in Figure 28

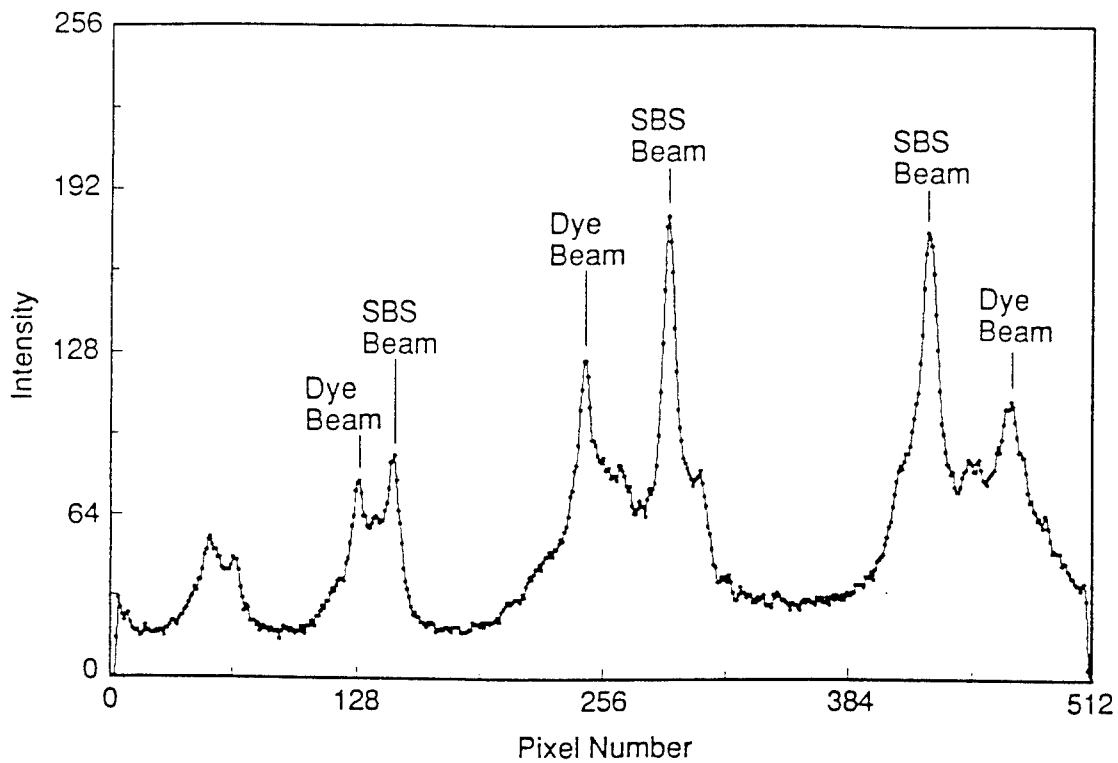


Figure 30. Reduced Data from F-P Images.

Figure 29 Data Transformed Into Wavenumber Space - Different Orders Overlaid

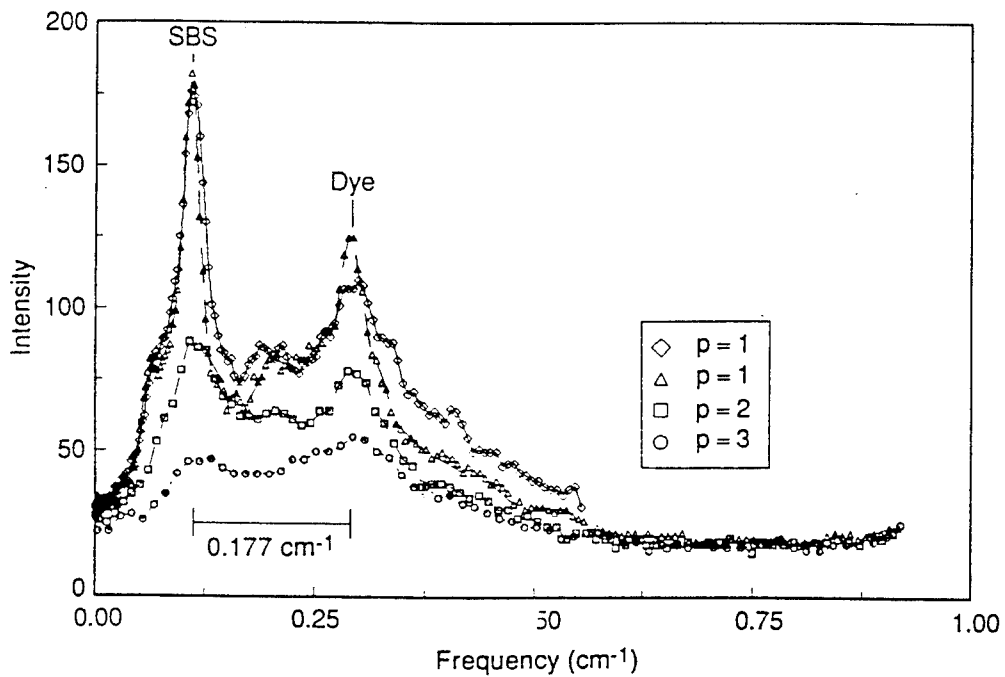
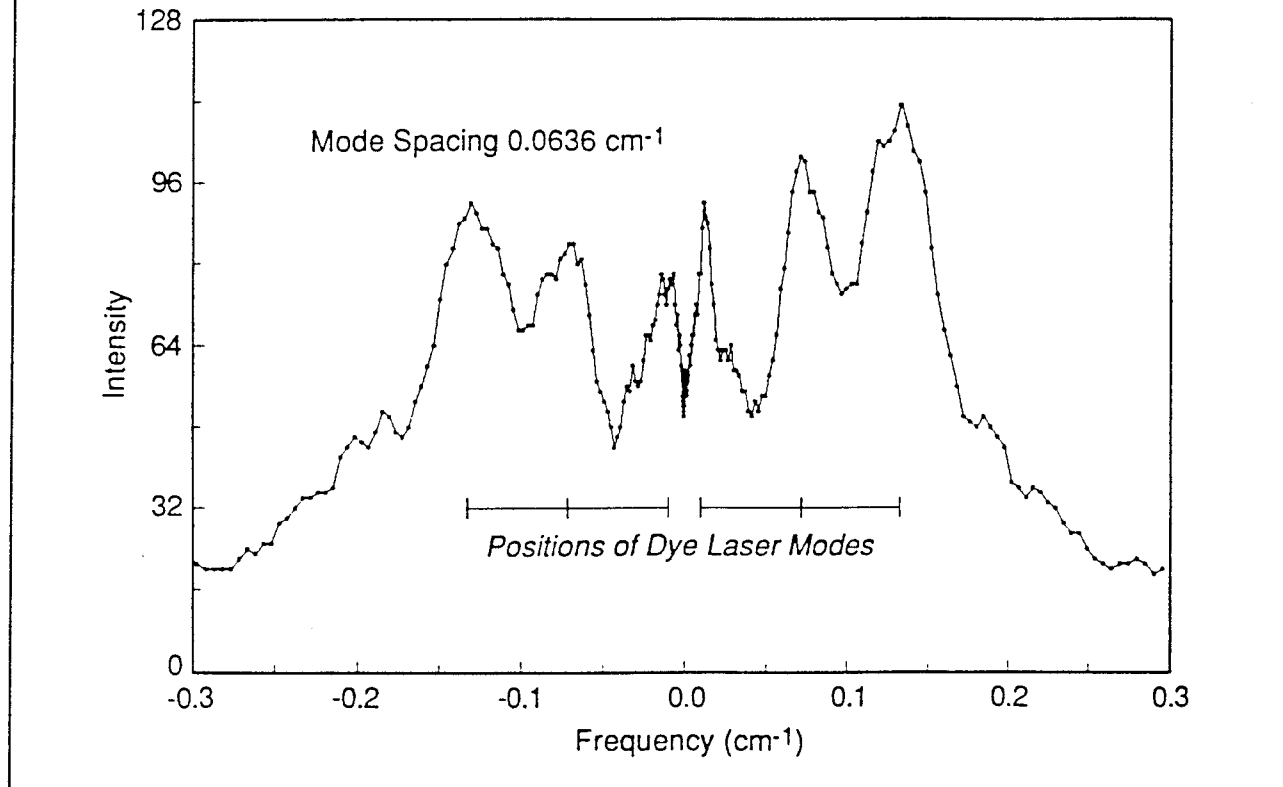


Figure 31. Interferogram Showing the Dye Laser Running in at Least 3 Axial Modes

The Mode Spacing is Indicated



Dye Laser Experiments:

The next set of measurements was concerned with the efficiency of the SBS mirror. We installed the optical isolator (Faraday rotator and two Glan-Taylor prisms) as shown earlier in Figure 26. This isolated the dye oscillator with its very sensitive optical components from the SBS back propagating beam. The operation of the optical isolator is as follows. The vertically polarized dye laser beam is transmitted through the first glan-Taylor prism (GP1 in Figure 26). The polarization vector is then rotated 45° by the Faraday rotator. The GP2 prism is configured to pass this polarization rotated beam. Upon reflection from SBS mirror, the SBS beam passes through GP2 and is rotated an additional 45° by the Faraday rotator. At this point the polarization of SBS beam is horizontal and is outcoupled by the GP1. With this protection the dye laser could be run at higher power levels. We examined several configurations similar to that shown in Figure 26 with the SBS cell external to the dye laser. We observed that SBS in methanol was produced for dye laser pulse energies as low as 2 mJ. Indeed, we were able to produce an SBS beam without pumping the final dye amplifier.

When dye was added to the methanol solution the SBS output was diminished by approximately 25%. However, this result should be considered preliminary since a systematic study of source of the diminution was beyond the scope of the program. One possible explanation for the reduction is absorption (albeit small) at the SBS wavelength by the R-590 dye in the SBS mirror cell.

We also tested a configuration that routed some of the green pump light outside the dye laser to excite the SBS cell. The output from the dye laser oscillator and preamplifier was amplified in this external cell and then focused back into the cell with a concave mirror. The SBS beam returned from the final amplifier cell and passed back through the amplifier once again prior to being outcoupled by the Faraday optical isolator. We learned from this external configuration one should avoid generating SBS in a volume of high optical gain. Any leakage of the dye beam through the SBS gain volume is amplified and produces a high power filamentary beam that damages the cell walls. Focusing the dye beam in the gain volume also produced significant amplified spontaneous emission (ASE). It was clear that these problems could be eliminated if the SBS volume and

the amplification volume were physically separated. Since one of our major program goals was to construct a cell that served as both the final dye amplifier and SBS mirror, we arrived at the design shown in Figure 32. The original Quantel dye laser amplifier was removed and replaced with the rectangular cell (Lambda Physik) described earlier. The rectangular cell was large enough to allow us to fold and focus the dye beam back into the amplifier cell. In addition, the Lambda Physik cell contains a metal shield that divides the cell into two halves. The 532 nm pump beam enters the front half, the final amplifier volume. The metal barrier blocks the 532 nm pump radiation from entering rear half of the cell, and in this region the dye solution is not optically excited by the pump radiation. The metal shield also allows the dye to circulate through both sides. Hence, the gain and the SBS volumes are easily separated from one another in a co-planar, folded geometry.

As indicated in Figure 32, we used a 7.5 cm focal length mirror to focus the beam exiting the final amplifier back into the "cold" side of the amplifier cell to establish the SBS mirror. We note that these modifications were necessary since the capillary tube final amplifier that the Quantel dye laser normally uses was not suitable for this purpose. The standard Quantel final amplifier diameter is only 5 mm and is side pumped by the 532 nm Nd:YAG laser. Consequently the entire volume of the cell was excited by the pump radiation and there were no unexcited or cold regions in the cell. When we attempted to focus the dye beam back into this amplifier, the optical gain in the tube caused strong, and uncontrollable amplified spontaneous emission (ASE). This can cause optical damage to the cell walls. Although programmatic constraints prevented a more thorough investigation, we concluded that if one uses the final amplifier cell for both a normal amplifier and the SBS mirror, then the volume to be used for SBS must be isolated from optical excitation by the pump

radiation. Design of this final cell to optimize SBS and dye powers are suggested as a critical area for future study.

We performed numerous tests designed to determine the efficiency of the SBS generation. These tests were completed by measuring both the dye and SBS beam energies using the configuration shown in Figure 33. Note that the dye beam was measured after one pass through the power amplifier, while the SBS made an additional pass through the amplifier. We attempted to construct an analogous two-pass amplifier for the dye beam. The concave mirror used to focus the dye laser for SBS generation was replaced by a flat mirror that reflected the dye beam back through the amplifier. This would have allowed direct comparison of SBS and two-pass dye beam energies, from which the SBS mirror efficiency could be determined. We found that this was a complicated procedure that produced unreliable results because it was extremely difficult to align the reflected dye beam back through the optical isolator. For this first set of measurements, we dismissed this approach and compared SBS pulse energies that made a second traversal of the gain medium to dye energies that made only a single pass through the amplifier.

In separate experiments, we measured the energy of the two beams as a function of the energy of the Nd:YAG pump beam. The energy/pulse was measured using a Scientech power/energy meter model 372. A plot of the SBS energy/pulse as a function of measured dye laser energy/pulse is shown in Figure 34. An SBS energy/pulse of 23 mJ was demonstrated.

During the power extraction experiments we observed what appears to be optical activity in the dye amplifier/SBS cell. Recall that we used a Faraday rotator sandwiched between two glan-Taylor prisms as an optical isolator. As discussed earlier, in its normal operating configuration, the first glan-Taylor

Figure 33. Experimental Configuration for SBS and Dye Laser Efficiency Measurements

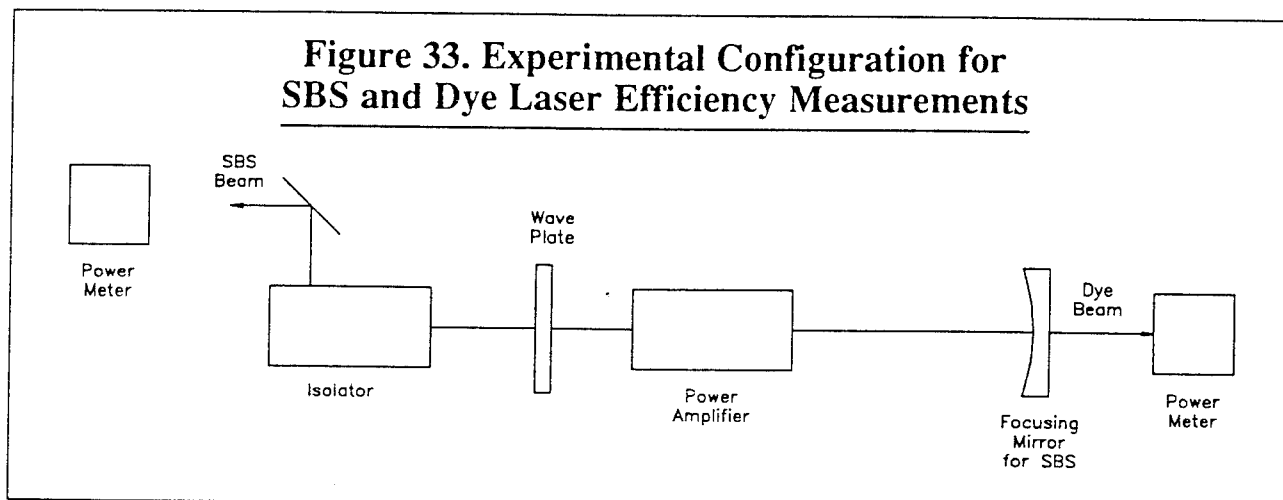
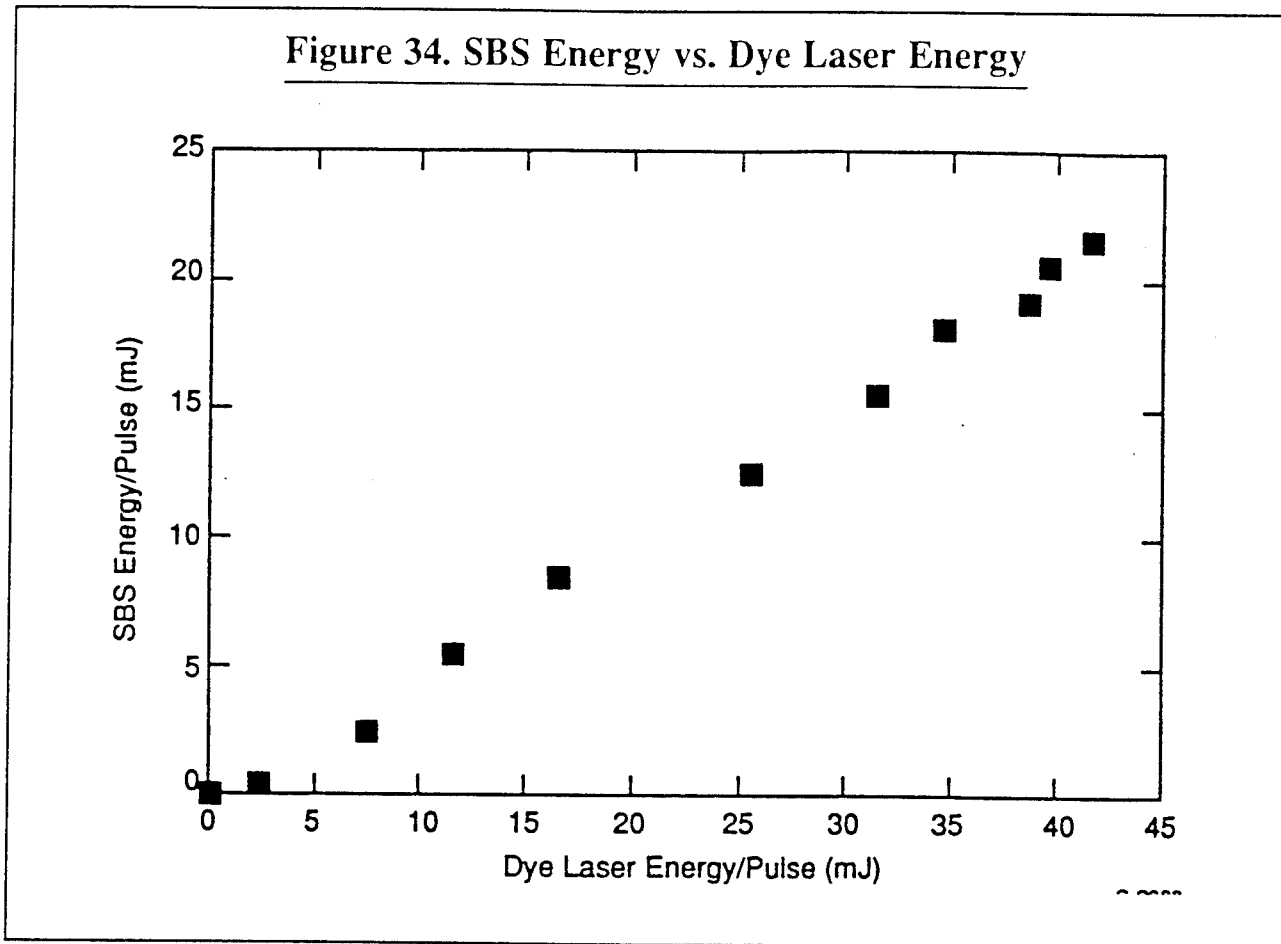


Figure 34. SBS Energy vs. Dye Laser Energy



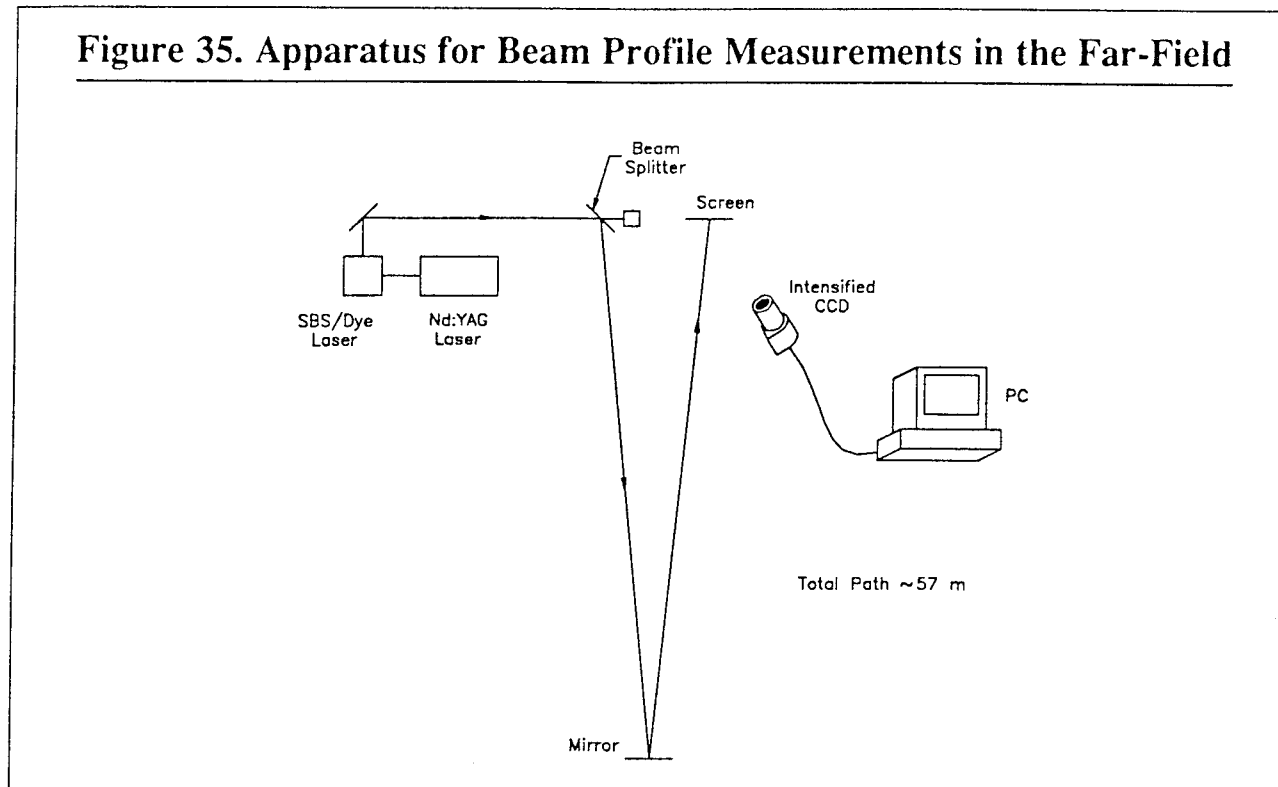
prism (GP1) passes the vertical polarization vector of the incident dye beam. The polarization is then rotated 45° by the Faraday rotator and the second glan-Taylor prism (GP2) is rotated to transmit this radiation. This beam then makes two traversals through the amplifier/SBS cell, and then passes back through the optical isolator. We expected that this counter propagating beam should be transmitted by the first glan-Taylor prism it encounters (GP2) then be rotated an additional 45° by the Faraday rotator, and finally be reflected out by the final glan-Taylor prism it encounters (GP1) since the polarization of the counter propagating beam is perpendicular to the polarization of the initial dye beam. However, we observed a significant fraction of the SBS beam was outcoupled by the glan-Taylor prism closest to the dye cell (see Figure 32) thus reducing the effective efficiency for the SBS process. This can only occur if the dye amplifier is an optically active (causes a rotation of the polarization vector of the dye beam). We surmise that the dye medium is being polarized by the strong 532 nm pump beam. Note that a 45° angle exists between the polarization of the 532 nm pump beam and that of the dye beam (as it enters the amplifier cell). If the 532 nm pump induces a polarization, some optical activity might be ex-

pected. More work to better understand this phenomenon is required.

We conducted several tests to compare the beam quality of the conventional dye laser output to that of the SBS dye laser. In practice, there are two methods for examining the far-field beam profile. One can use a high quality lens to focus the laser beam. At the focus the beam is transformed into the far-field limit. While this is a convenient method to assure that the far-field profile has been attained, the geometrical size of the focused spot would have been too small. We would not have been able to illuminate a sufficient number of pixels on the CCD camera and this would have resulted in poor spatial resolution.

The alternate method is to allow the beam to propagate a distance sufficient to transform into the far-field. A larger beam profile results since the beam is not focused. This is the approach that we used for the beam profile measurements. The set up for these propagation tests is indicated in Figure 35. Both outputs from the dye laser (dye beam and SBS beam) were propagated 57 m using a series of prisms and mirrors. At the end of the propagation length, the beams were incident on a white screen. The beams could be readily examined visually on a

Figure 35. Apparatus for Beam Profile Measurements in the Far-Field



single-shot basis. Typically the spot diameter was about 2 cm on the screen.

We recorded single shot images of the beam profiles on the screen using an intensified CCD camera. Typical images for both the dye beam and the SBS beam are shown in Figures 36 and 37, respectively. A look-up table for the false color encoding is indicated in each figure. The 26 colors each cover 10 A/D levels. Consequently, the full dynamic range in any one figure is approximately 250. The SBS image contains a circular bright region, which we observed in all the SBS images that we recorded.

In contrast, the beam profile images for the dye laser output were highly aspherical as indicated in Figure 37. Investigation of the details concerning why the dye beam appeared this way was beyond the scope of our program. We feel confident that a major contributor is the side pumped geometry of the dye laser preamplifier and final amplifier resulting in a highly nonuniform gain profile and a thermally induced wedge. In the modification of the Quantel dye laser, we used a rectangular final amplifier that was side pumped by the Nd:YAG laser. In this configuration the Nd:YAG laser beam is formed into a sheet using cylindrical optics. The dye mixture in the final amplifier absorbs the dye beam in only a few millimeters. This gives rise to a non-uniform gain profile with the gain highest at the edge of the dye cell. The dye preamplifier has a similar profile. Often in dye lasers this results in a triangular beam profile. Notable examples are excimer and Nd:YAG

pumped systems. To enhance the beam quality some dye laser manufacturers use side pumped, thin cylindrical final amplifiers or pump the final amplifier longitudinally. As we discussed above, these options were not feasible with the dye system that was available for this effort.

The digitized images such as shown in Figures 36 and 37 were analyzed to obtain the intensity profiles by examining cuts through the centers of the images. In Figures 38 through 41 we show examples for horizontal and vertical cuts through the images in Figures 36 and 37. The beam profile of the SBS beam is clearly superior. Inspection of Figures 38 and 39 reveals that the average divergence for the SBS beam in the horizontal and vertical planar is $255 \mu\text{rad}$. The diffraction limit is defined as $1.22 \lambda/d$ where λ is the wavelength (563 nm) and d is the diameter of the final aperture at the SBS output (4 mm). The diffraction limit is thus $171 \mu\text{rad}$, and the SBS beam divergence is ~ 1.5 times this value. The SBS beam is close to diffraction limited, and can therefore be focused to a small size with an excellent intensity profile. One of the important implications of this work is that non-linear frequency conversion such as doubling, tripling, or parametric oscillation could be more efficiently performed than in non-phase-conjugated systems.

Finally, in Figures 42 and 43 we display 3-dimensional plots of the far-field beam profiles presented in Figures 36 and 37. The dramatic improvements in the SBS beam are obvious.

Figure 36. Photograph of Single Shot Digitized Image of SBS Beam in Far-Field



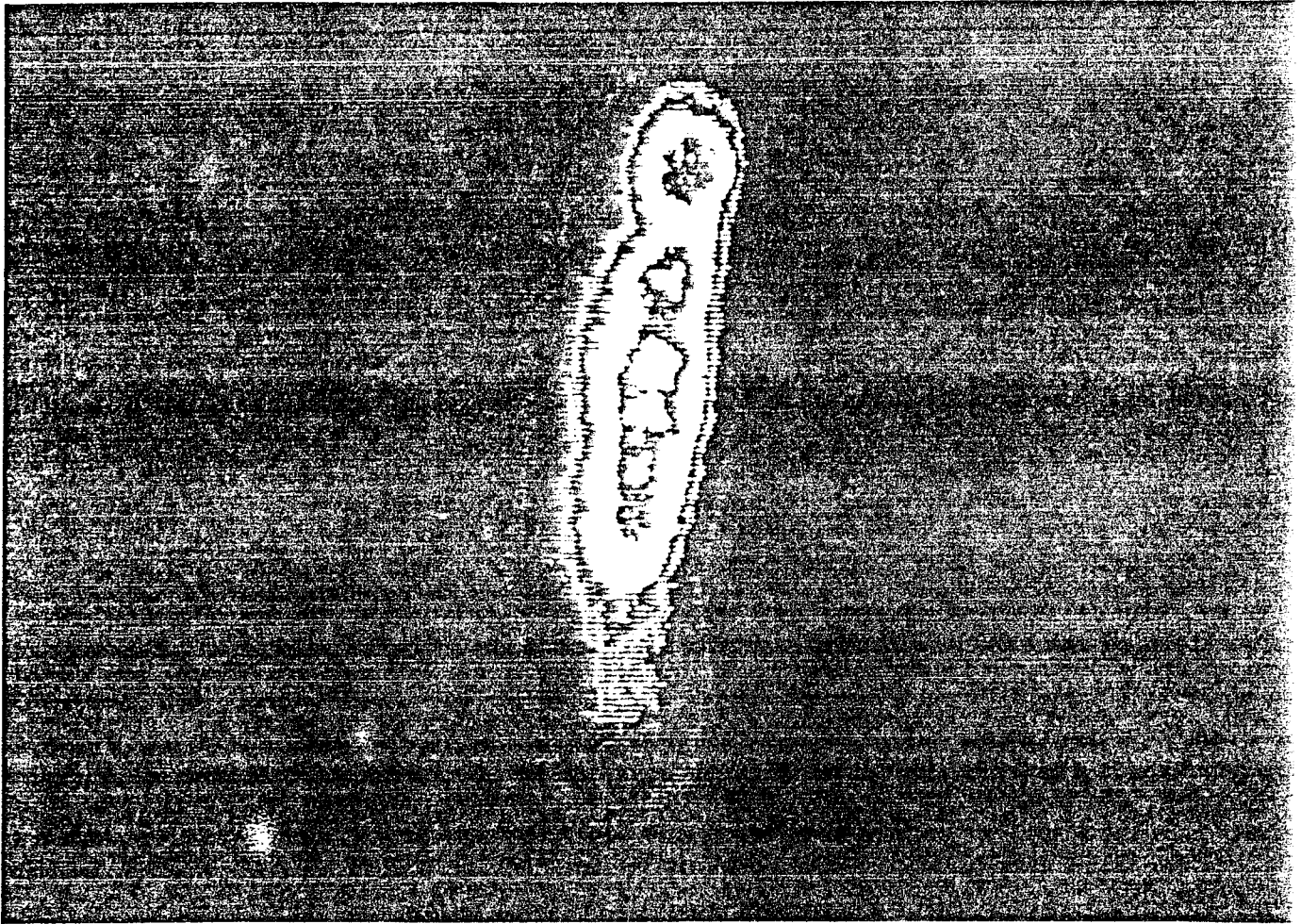
We also monitored the long-term stability of the dye/SBS laser output. A single dye charge was used for both the oscillator/preamplifier and power amplifier dye solutions. The oscillator/preamplifier Rhodamine 590 dye solution concentration was 2.5×10^{-4} moles/liter. The power amplifier Rhodamine 590 dye solution concentration was 1.5×10^{-4} moles/liter. These solutions were pumped by approximately 10^5 , 400 mJ, 532 nm laser shots at a 10 Hz repetition rate over a six month period of time. We observed no loss of energy or conversion efficiency due to focusing the dye laser output into the power amplifier for SBS mirror creation over this time period. The laser dye solutions maintained a constant color and displayed no signs of degradation; spectral confirmation was not performed due to the fact that the laser output was consistent. This indicates that the SBS medium lifetime was not degraded over the time frame and energy deposition rate tested in this program.

Dye Laser Demonstrations:

The entire laser system was first demonstrated in late May 1992. Due to other programmatic obligations for the dye laser, the laser was returned to PSI and subsequently returned to LTA for the second and final demonstration that took place in October 1992. In each of the two demonstration series, the SBS/dye laser was mated to the LTA frequency doubled Nd:YAG laser and a series of demonstration tests were performed for Dr. Carol Pearce, the Army technical monitor. These tests included efficiency measurements, wavelength tuning of the SBS/dye laser, and some beam quality measurements.

During the May 1992 demonstration the pulse energy of the green pump laser was 60 mJ at 10 Hz repetition rate. A block diagram for the experimental arrangement is given in Figure 44. In Figure 45 we present plots for both the dye laser energy and SBS energy as a function of the wavelength of the dye laser. Two runs for the SBS are indicated. At most

Figure 37. Photograph of Single Shot Digitized Image of Dye Beam in Far-Field



wavelengths the dye SBS output energy was between 40 and 60% of that for the dye, consistent with the earlier tests at PSI. We again note that for these measurements the dye beam made only one pass through the dye cell while the SBS beam made a second pass.

We also demonstrated improvements in the beam quality of the SBS beam versus the dye beam. Burn patterns of both beams were provided to Dr. Carol Pearce. The areas of the SBS burns were several times smaller than those for the dye beam. Since these burn patterns were not obtained in the far-field, they are not as relevant as the data presented in Figures 36 and 37. A more complete set of beam diagnostics in the far-field was recorded during the October 1992 demonstration. These data are presented below.

During the second demonstration of the PSI SBS/Dye laser that was pumped by the LTA Phase II Nd:YAG laser, a series of experiments was undertaken to record pump laser energies, dye laser and

SBS dye laser energies, efficiencies, far-field beam quality, laser beam jitter and laser pulse temporal profiles. The far-field beam quality and beam jitter measurements were recorded during the laser demonstration for Dr. Carol Pearce, the Army technical monitor.

The energy measurements recorded are presented in Table 1 and provide information on the 532 nm pump beam energy distribution within the dye/SBS laser and the dye and SBS laser output energies. Note that the pumping losses in this commercial dye laser are rather large, and that an immediate 12% increase in laser efficiency could be achieved by using AR-coated optics (532 nm). The overall dye laser energy efficiency of 5.1% with SBS is also low, however this is again attributable to the use of the lossy unoptimized commercial dye laser. The elimination of uncoated optics and the preamplifier, and further optimization will increase efficiency to 30-35% for narrowband operation with SBS.

Figure 38. Horizontal Slice Through SBS Beam Image from Figure 36

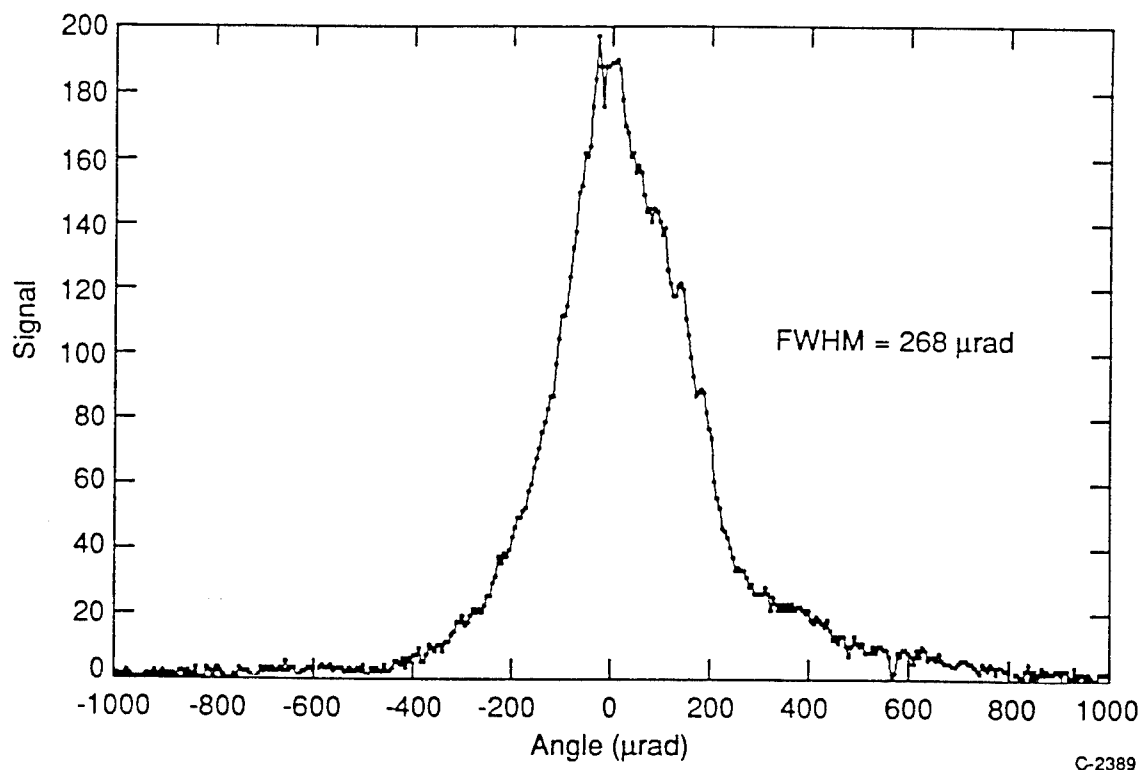


Figure 39. Vertical Slice Through SBS Beam Image from Figure 36

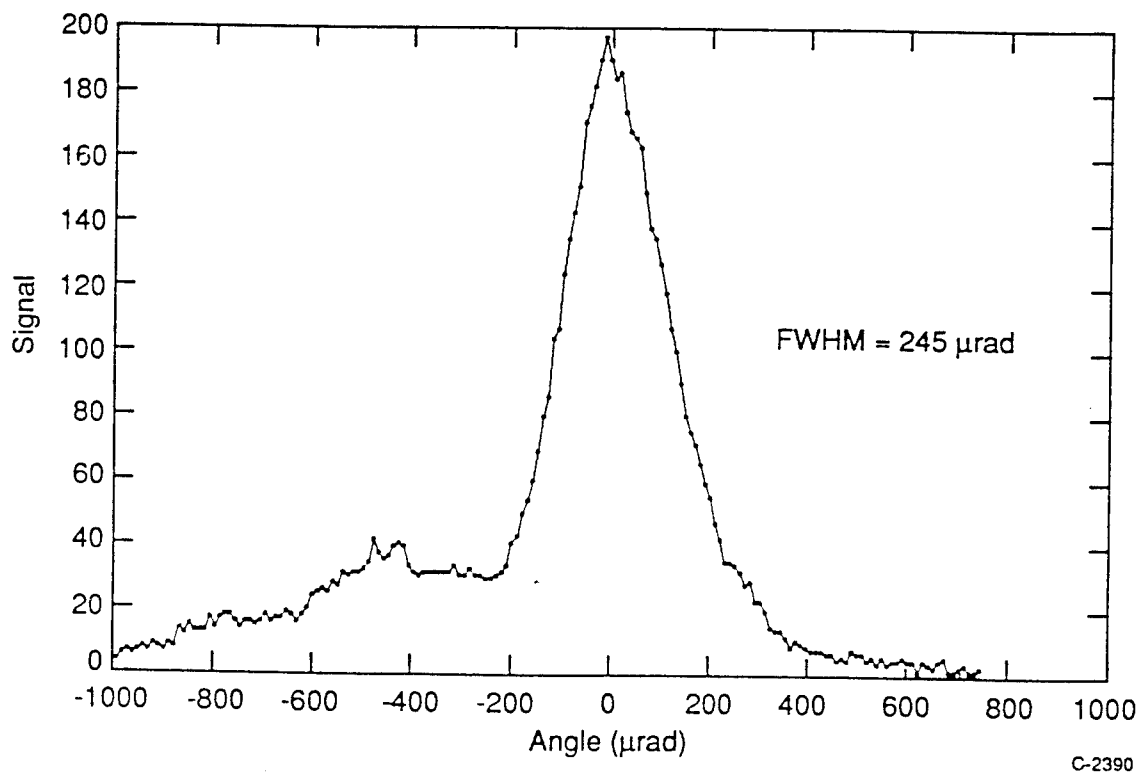


Figure 40. Horizontal Slice Through Dye Beam Image from Figure 37

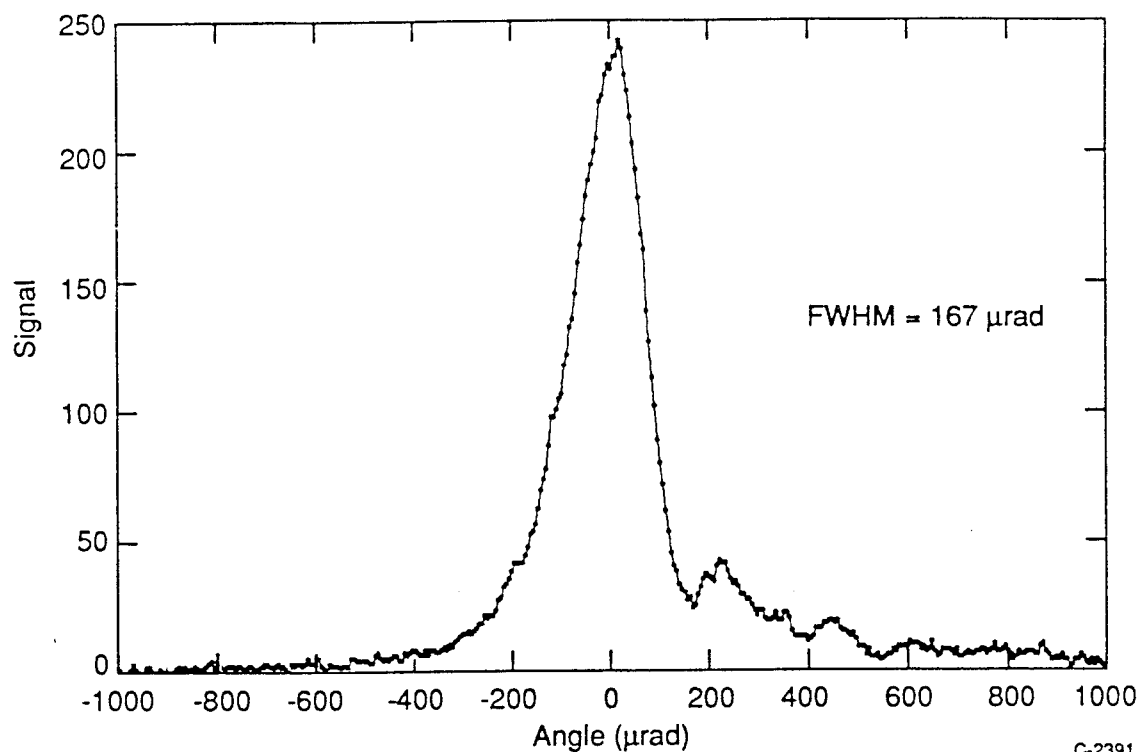


Figure 41. Vertical Slice Through Dye Beam Image from Figure 37

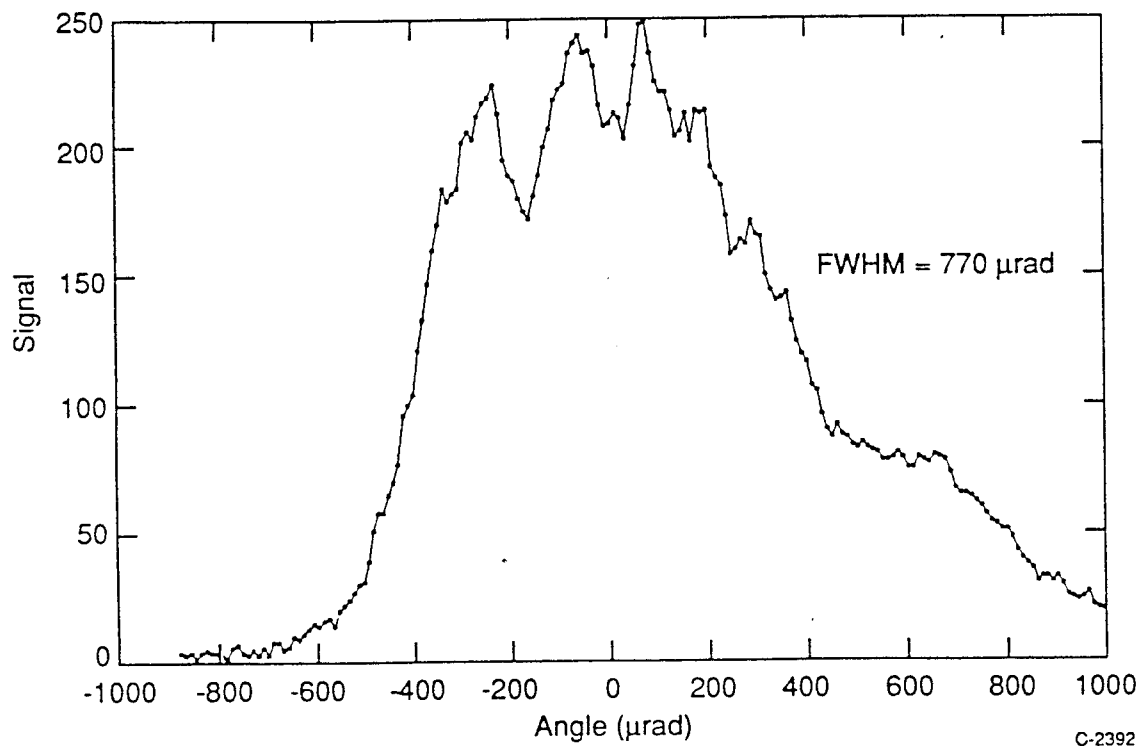


Figure 42. Far-Field Profile of SBS Beam Obtained from Figure 36

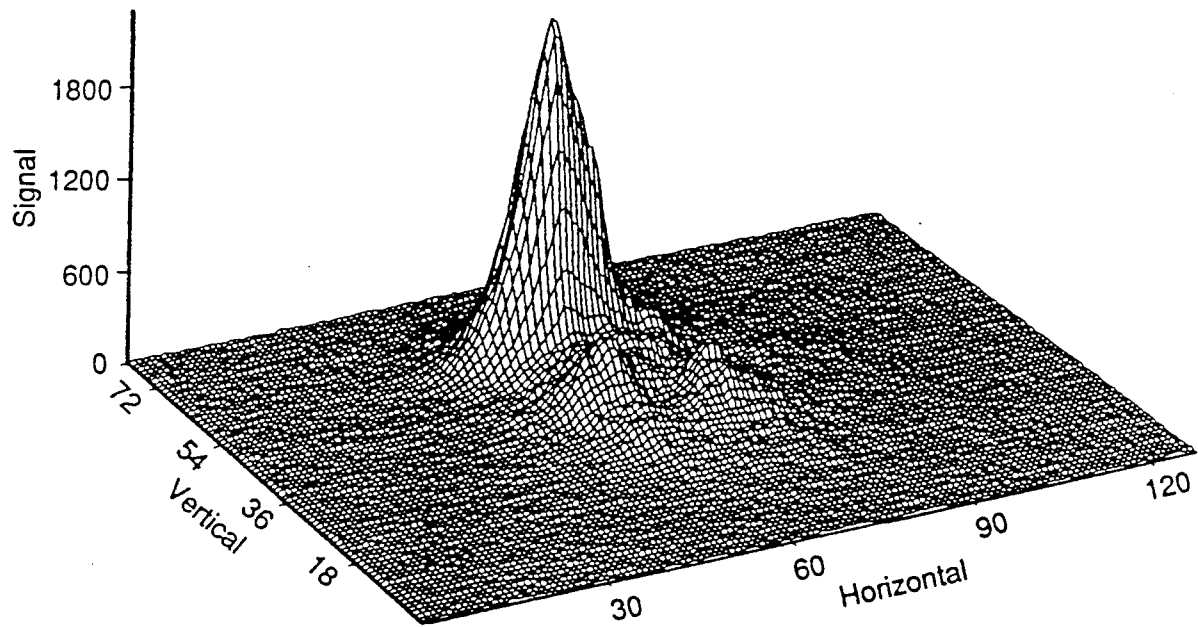


Figure 43. Far-Field Profile of Dye Laser Beam Obtained from Figure 37

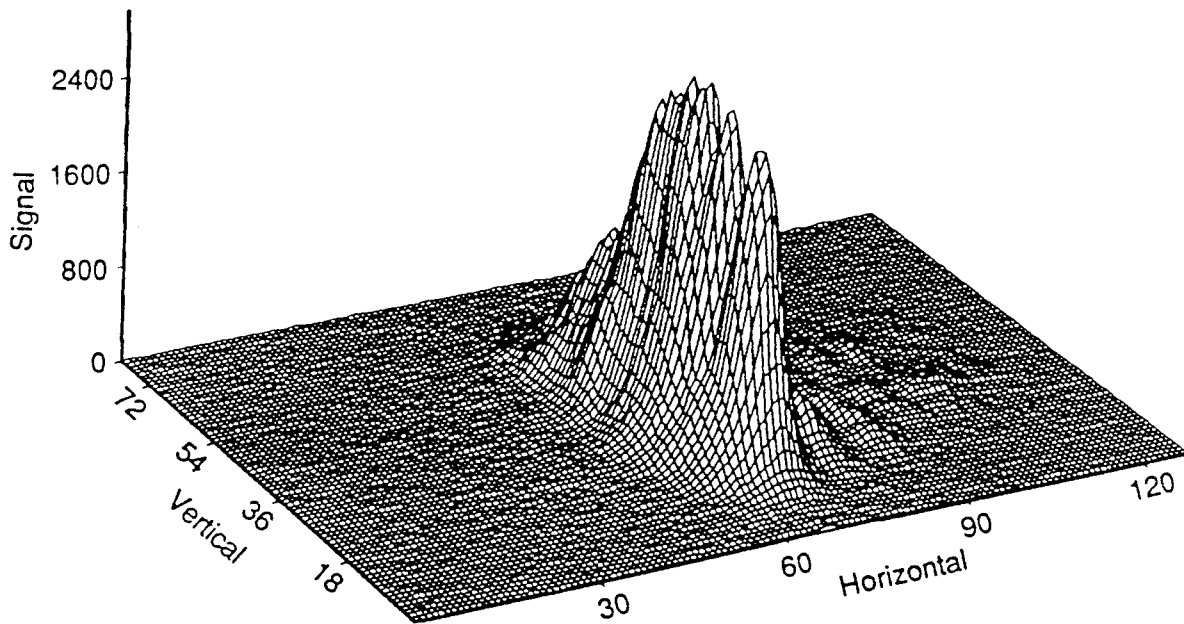


Figure 44. Block Diagram for Initial Tests Performed at LTA

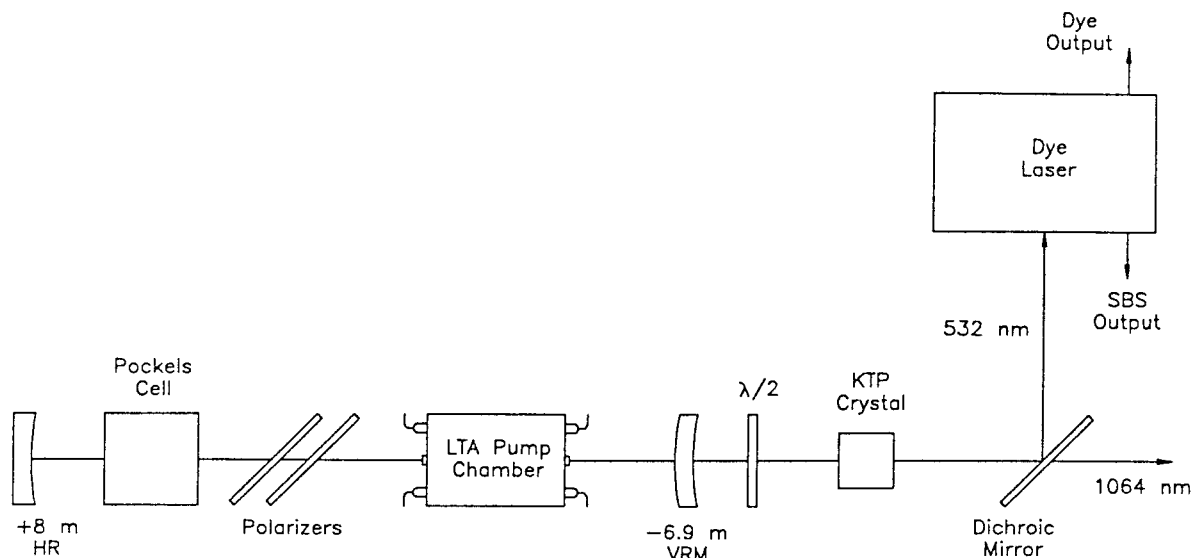
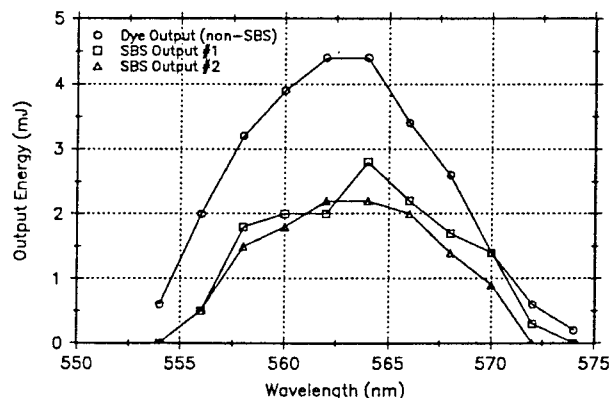


Figure 45. SBS and Dye Laser Energy vs. Dye Wavelength

Constant Pump Energy (532 nm) of 60 mJ/Pulse at 10 Hz



The dye laser output energy after the first pass of the power amplifier was 9.5 mJ/pulse. The double-pass amplifier energies were recorded under two different configurations. In the first configuration a flat mirror was positioned after the amplification. The beam was outcoupled via the optical isolator. This configuration resulted in 10.2 mJ/pulse of output energy. Thus, the second pass of the power amplifier resulted in only a 7% rise in the output energy, implying that more than 90% of the energy available was swept out on the first pass through the amplifier. In the second configuration the single pass dye laser beam was focused by a concave mirror into the "cold" region of the power amplifier. The resulting SBS beam reflected off of the focusing mirror and

back through the power amplifier. Once again the SBS beam was outcoupled via the optical isolator. This configuration resulted in 4.1 mJ/pulse of output energy. Thus the SBS mirror efficiency was approximately 40%. It should be emphasized that the SBS efficiency was in fact closer to 50% due to the optical losses in the system. These could be eliminated by using coated rather than the uncoated optics used in our experiments.

During an additional set of experiments, an optical quartz flat was placed at 45° between the final power amplifier and the SBS focusing mirror. This setup allowed us to directly measure the reflectivity of the SBS mirror created in the dye cell by comparing the focused and reflected beam energies. We

Table 1. Phase-Conjugated Dye Laser Energy Partition

Pump Laser (532 nm)	
At Input (10 Hz):	80 mJ
At Oscillator:	6.25 mJ
At Pre-amplifier:6:	6.25 mJ
At Double-Passed Amplifier:	58 mJ
Loss in Optics:	9.5 mJ
Dye Laser (570 nm)	
Oscillator Output:	0.2 mJ
Pre-amplifier Output:	0.75 mJ
Double-Passed Amplifier (570 nm)	
First Pass:	9.5 mJ
Second Pass:	
Flat Mirror:	10.2 mJ
SBS mirror (Phase-Conjugated):	4.1 mJ
40% SBS Efficiency	

recorded a mirror efficiency of $30\% \pm 10\%$. These measurements are more difficult to record than the previously described efficiency measurements due to the low energy levels reflected by the 45° quartz flat. We believe this measurement is consistent with our previous determination of a 40% SBS mirror efficiency.

We note that both of the efficiency measurements recorded during the second SBS laser demonstration

are lower than the measurements recorded during the first laser demonstration. This difference is due to the double pass amplification of the dye laser beam during the second set of measurements as opposed to the single pass measurements of the first demonstration.

In Figure 46 we show the dye laser output temporal pulse shape for a single pass of the final dye amplifier, a double pass with retro mirror, and double passed with SBS. As expected, the single and double passed with ordinary mirror have about the same pulsewidth (10.00 and 10.94 nsec FWHM, respectively), due to the fact that most amplification takes place on the first pass. The SBS pulsewidth however, is significantly less (8.40 nsec FWHM), primarily due to the characteristically sharper rising leading edge and pulse compression associated with the nonlinear SBS process.

Also, during the final demonstration, we measured the dye laser output beam quality, beam jitter, and pulse width. In Table 2 we show the beam quality measurements for the dye laser with the final amplifier double-passed with an ordinary (retro) and a phase-conjugate (SBS) mirror. It can be seen that, in the horizontal direction, the beam-quality improved from 5.55 to 2.25 mm-mrad, and in the vertical axis, from 2.17 to 1.80 mm-mrad. Note that the larger improvement is found in the horizontal axis where non-uniform transverse pumping is operative which will degrade beam quality.

To make the beam quality measurements, we propagated the dye output beam a distance of 7.34 m (from the minimum waist) and, using our video imaging equipment, took a number of shots (four each with the retro and SBS mirrors) of the propagated beam. By calibrating the camera spatially (pixels per millimeter), we calculated the $1/e^2$ widths of the beam in the horizontal and vertical axes. We found (and measured) the (minimum) waist of the propa-

Figure 46. SBS and Dye Laser Beam Temporal Pulse Shapes

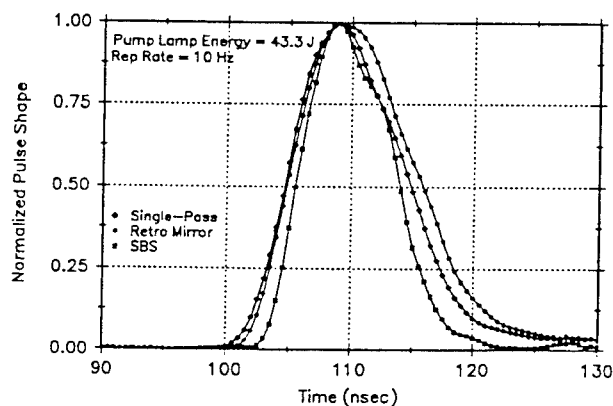


Table 2. Dye Laser Beam Improvements with SBS

	Retro Mirror	SBS Mirror	Units
Beam Quality:			
Horizontal Axis	5.55	2.25	mm-mrad
Vertical Axis	2.17	1.80	mm-mrad
Output Pulse Energy	10.2	4.1	mJ
Pulsewidth	10.94	8.40	nsec
Peak Power	932.4	488.1	kW
Peak Brightness	6.08	9.47	$\times 10^{12}$ W/cm ² -Sr
Beam Jitter (Standard Deviation):			
Horizontal Axis	617	167	μ rad
Vertical Axis	225	170	μ rad

gated beam using burn paper. By knowing these two sets of data, we calculated the beam divergence and, thus, beam quality. The beam quality data in Table 2 is the average for the four sets of shots for both mirror cases. In Figure 47 we show an example of the beam profiles of the dye laser output beam with the retro mirror and SBS. It is significant to note the single peak found with the SBS beam and multiple (spread out) peaks with the retro mirror.

Further on in Table 2, we show the calculated beam brightness for the retro and SBS mirror cases. Beam brightness is a very important parameter for calculating beam propagation and expected intensity on a target. It incorporates both the beam power and beam quality into a single quantity. Peak beam brightness, B_{PK} , is defined as

$$B_{PK} = \frac{P_{PK}}{BQ_H BQ_V} \frac{\pi}{4} \times 10^8 \quad (2)$$

where BQ_H and BQ_V are the horizontal and vertical beam quality values (in mm-mrad), respectively, and P_{PK} is the peak power (W). B_{PK} is in the units W/cm²-Sr. The constant term in eqn. (2) accounts for the conversion of (mm-mrad)² to cm²-Sr.

Note that even though the pulse energy for the SBS mirror is only 40% of that with the retro mirror, the brightness is 56% greater with SBS. This result is mostly due to the improved beam quality produced with SBS in addition to some pulse compression also produced with SBS. A beam with higher bright-

ness will generate higher intensity on target. This shows quite evidently the importance of the use of the SBS mirror in overall system performance.

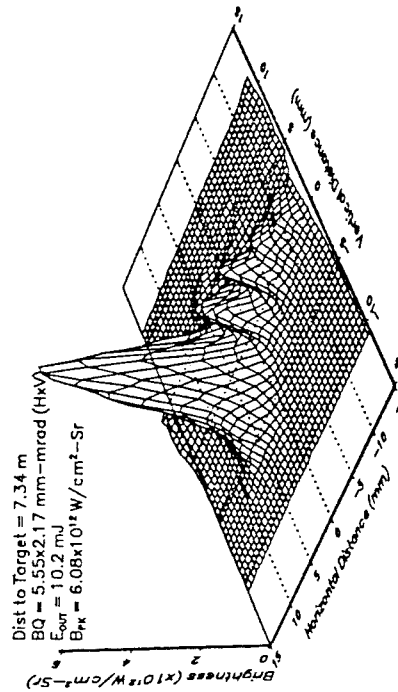
In Figure 48 we show the measured beam angular jitter in both the vertical and horizontal direction. The standard deviation of the data is also drawn for comparison. (These are also tabulated in Table 2.) Beam jitter was measured in a similar method as beam quality by imaging the dye and SBS beams at a distance from the final laser output mirror. We again processed the images (8 each for the retro and SBS mirror cases) with our video processing software to determine the centroid of the beam for each case. By calibrating the camera spatially, we determined an average spatial position and (lateral) distance from that position or spatial jitter. This was converted to angular jitter by simply dividing by the range to the image target. The decrease of beam jitter with SBS, from 617 to 225 μ rad in the horizontal direction, is dramatic. No improvement is seen in the vertical direction, as expected. Beam jitter is important in determining intensity on target. Jitter effectively smears out the beam from shot to shot thus reducing beam intensity on target.

During this final demonstration, the repetition rate of the 532 nm pump laser was increased from 10-18 Hz, limited only by the laser power supply. Approximately 65 mJ of 532 nm light was used to pump the dye laser. No deterioration in the SBS output nor beam quality was detected.

Figure 47. Dye Laser Output Profiles

Beam Brightness Profiles After Propagating 7.34 m

**Double-Pass Amplifier
With Retro-Mirror**



**Double-Pass Amplifier
With SBS**

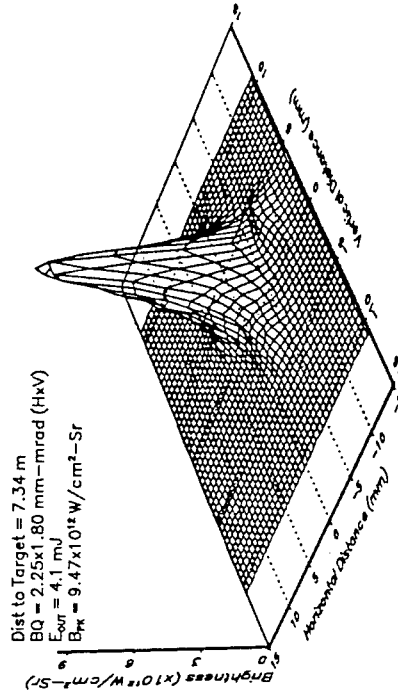
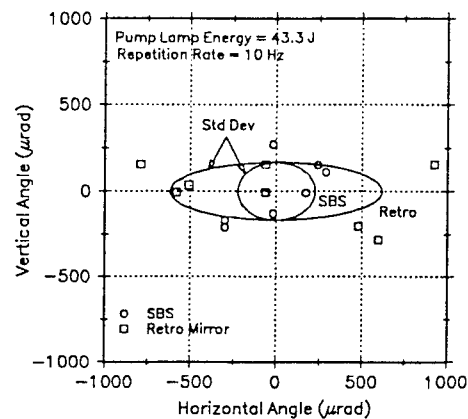


Figure 48. Scatter Plot of Dye and SBS Laser Beam Center Points



VI. Summary and Recommendations for Phase III

The work performed in this contract has proven the viability of an SBS dye laser in a commercial platform capable of producing near diffraction limited beam quality in the far-field. We believe this is an important demonstration with positive implications for Army missions and commercial development. By incorporating the SBS in the final double pass amplifier, we were able to increase beam brightness by almost 60% over the use of an ordinary retro mirror. This increase in beam brightness is despite a decrease in energy efficiency. The loss in energy efficiency is more than made up in the improved beam quality produced by using SBS. It should be noted that we were only able to achieve 40-50% reflectivity from the SBS mirror; reflectivities as high as 80% have been demonstrated indicating that a further increase in beam brightness is possible. The SBS process also decreased beam jitter by a factor of 2.74. Beam jitter results in an effectively larger propagated spot. The combined increase in beam brightness and decrease in jitter result in significantly higher performance for the SBS dye laser system.

However, the scope of this program did not allow investigation of a number of scientific issues which arose during these demonstrations. The overall efficiency of the dye laser and the SBS efficiency were relatively low. In the following we address these issues and describe potential solutions which would result in a higher efficiency SBS dye laser.

The commercial dye laser platform which was reconfigured into the SBS/dye laser was a high-resolution spectroscopic instrument. The Quantel TDL-50 produces a narrow frequency bandwidth laser beam with excellent beam quality in the near-field. These two spectroscopic attributes are

achieved at the expense of high conversion efficiency. For example, due to a beam expanding telescope, less than 50% of the dye laser oscillator beam traverses the preamplifier cell. Similarly, approximately 50% of the amplified portion of the oscillator beam which exits the preamplifier cell overfills the final power amplifier. These seemingly inefficient configurations are used to improve beam quality. The typical output of the TDL-50 running on Rhodamine 590 laser dye, pumped by 500 mJ of 532 nm radiation is 100 mJ. This translates into only a 20% conversion efficiency.

Due to the need to protect the dye laser oscillator from the SBS laser beam, the optical isolator was added to the dye laser prior to the final amplifier. The clear aperture of the isolator was only 4 mm, resulting in an 80% reduction in transmission of the oscillator/preamplifier laser beam. The second change to the original dye laser design involved the replacement of the capillary power amplifier dye cell with a rectangular dye cell as described above. This resulted in two effects: less efficient amplification and degraded beam quality. The combination of these two significant modifications to the dye laser resulted in a 12% overall conversion efficiency for the single pass amplifier dye laser. These two changes were critical to the successful demonstration of the SBS dye laser, but were not designed for optimum conversion efficiency since we were constrained to work with the available commercial Quantel dye laser.

Significant improvements in the performance and efficiency of the dye laser can be made with further work. Improvements can be made in the efficiency of the SBS mirror. Several factors contributed to a less than maximum efficiency in the reflectivity of

the SBS mirror. First, as described earlier, we observed that the presence of laser dye in the methanol resulted in lower mirror efficiency. A lower dye concentration in the amplifier/SBS cell may have resulted in both improved dye laser beam quality and potentially higher SBS mirror efficiency. The scope of our effort did not allow a parametric examination of SBS efficiency versus dye concentration. The second factor which limited the SBS mirror efficiency stemmed from difficulties in focusing the dye laser beam into the flowing dye cuvette. We observed some self focusing of the dye laser beam in the dye doped methanol solution. This effect in combination with the focusing mirror used after the amplifier cell to create the SBS mirror, resulted in a compound lens pair with a degraded focusing ability. The reduced power density within the flowing dye cell reduced the efficiency of the SBS mirror.

Minor impurities in the SBS medium may also have contributed to degradation in the SBS mirror. For example, methanol is known to absorb atmospheric water vapor, and the presence of water has been shown to reduce the SBS mirror efficiency [10]. A simple system to seal or purge the atmosphere above the laser dye solutions could eliminate the water contamination. Recently, Eichler and co-workers [11] reported significant increases in the efficiency of SBS in liquids when minute, undissolved particles were removed by repeated vacuum distillation. For example, the SBS efficiency in methanol was increased from approximately 1% to 10% following the distillations. For these studies Eichler et al. [11] used 100 mJ of broadband 1.06 μm radiation as the SBS generation beam. In addition, optical breakdown, sparking and bubble formation, all of which degrade SBS were reduced. Although we carefully filtered the dye solutions, no purification of the methanol was performed. This should also be investigated more thoroughly. The efficiency and output of the phase-conjugated dye laser remained constant over a six month period during which 10^5 laser shots were fired at the 400 mJ/pulse (532 nm) pump level. This indicates that the dye was not degraded by the pump light nor the SBS process.

The dye laser efficiency and SBS efficiency can be significantly improved with a newly designed dye laser. Computer modeling of the dye laser beam focus within a dye doped methanol solution would be used. The dye laser efficiency could be improved by first determining the bandwidth requirements for efficient SBS mirror production. If a broader bandwidth dye laser oscillator could be used to produce an efficient SBS mirror, then a significantly more efficient oscillator could be designed to provide this radiation. There will be a tradeoff between bandwidths of the dye laser and SBS efficiency since it is known that broadband lasers (low temporal coherence) produce degraded SBS. On the other

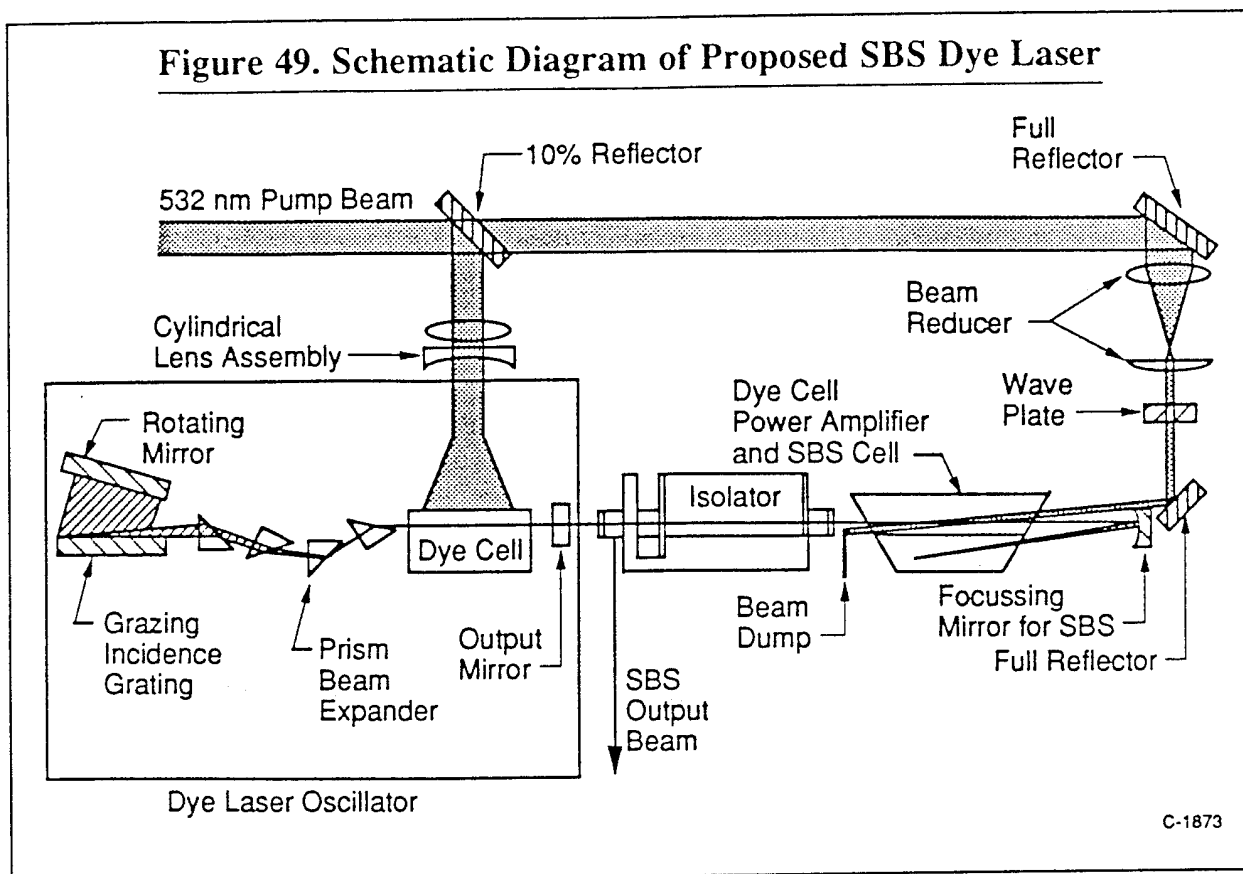
hand, higher efficiency dye lasers result if fewer laser line narrowing elements are used in the dye laser. The design of a more efficient amplifier optical train would result in high beam quality, yet efficient conversion would also be undertaken. The use of a divided capillary cell power amplifier would be employed to produce efficient amplification, improved medium quality, and the required environment for efficient SBS mirror production. A preliminary design is shown in Figure 49. Note that in this configuration the power amplifier is end pumped rather than side pumped. We believe that end pumping would result in a higher quality output beam. The configuration might also alleviate some of the polarization rotation observed in the side-pumped system described above.

Additional improvements in the dye laser design which would result in more efficient conversion are listed below:

- AR coated preamplifier cell
- AR coated power amplifier cell
- AR coated dye laser telescope
- AR coated Nd:YAG beam steering optics
- Large aperture optical isolator to avoid beam clipping

We believe that by implementing the aforementioned improvements to the dye laser we could achieve conversion efficiencies 30-35% for a Rhodamine 590 lasing medium with SBS used in the double pass amplifier. Furthermore, high repetition rate performance to the 40-50 Hz level could be achieved. The maximum repetition rate of 18 Hz demonstrated during this program was limited only by the power supply.

PSI and LTA are uniquely qualified to develop the SBS dye laser. PSI and LTA have extensive experience in laser development and laser characterization. In recent years PSI has developed the capability to accurately measure dye laser spectral mode structure and bandwidth on a single shot and average basis. PSI has experience in modifying dye lasers to tailor the output bandwidths for specialized programs and has achieved the desired laser characteristics for a number of programs involved in gas flow-field characterization. This capability will be essential in determining the effect of mode structure and bandwidth upon SBS mirror efficiency. LTA personnel have broad applicable experience with the characterization and use of SBS in removing system optical aberrations. PSI has also developed a powerful gain measurement tool capable of measuring optical gains below 10^{-6} . This capability has proven valuable for both dye laser and gas phase laser development. PSI and LTA have also been working



on laser dye characterization including IR laser dyes and alternative dye laser pumping schemes. LTA has extensive experience in optical resonator development and modeling using computer ray tracing codes. This experience would prove invaluable for

efficient dye laser development. The combined capabilities of these two organizations would result in an efficient development program to build an advanced compact SBS dye laser capable of tunable, near diffraction limited beam quality in the far-field.

VII. References

- [1] D.P. Benfey, R.E. Boyd, D.C. Brown, and D.J. Harter, "Laser Pump Chamber Optimization: Raytrace Modeling and Optimization Algorithm," *OSA Proc. on Tunable Solid State Lasers*, **5**, 392-396 (1989).
- [2] R.E. Boyd, J.W. Kuyper, and D.J. Harter, "Laser Pump Chamber Optimization: Modeling and Experimental Verification of Absorption in Biaxial, Trichroic Media," *OSA Proc. on Tunable Solid State Lasers*, **5**, 385-391 (1989).
- [3] H.T. Powell, A.C. Erlandson, and K.S. Jancaitis, "Characterization of High Power Flashlamps and Applications to Nd:Glass Laser Pumping," *Proc. of SPIE*, **609**, 78-94 (1986).
- [4] B. Ya. Zel'dovich, V.I. Popovichev, V.V. Ragul'skii, and F.S. Faizullov, *JETP Lett.*, **15**, 109 (1972).
- [5] D.A. Rockwell, *IEEE J. Quantum Electron.*, **24**, 1124 (1988).
- [6] M.R. Osborne, W.A. Schroeder, M.J. Damzen, and M.H.R. Hutchinson, "Low-divergence Operation of a Long-pulse Excimer Laser using a SBS Phase Conjugate Cavity," *Appl. Phys. B*, **48**, 351-6 (1989).
- [7] M. Slatkine, I.J. Bigio, B.J. Feldman, and R.A. Fisher, "Efficient Phase Conjugation of an Ultraviolet XeF Laser Beam by Stimulated Brillouin Scattering," *Opt. Lett.*, **7**, 108-10 (1982).

- [8] H. Meng and H.J. Eichler, "Nd:YAG Laser with a Phase-Conjugating Mirror Based on Stimulated Brillouin Scattering in SF₆ Gas," *J. Opt. Soc. of Amer.*, 569, (1991).
- [9] T.A. Wiggins, R.V. Wick, N.D. Foltz, C.W. Cho, and D.H. Rank, "Optical Mixing in Stimulated Brillouin Spectra," *Opt. Lett.*, 16, 569 (1991).
- [10] D. Brown, Laser Technology Associates, Inc., Johnson City, New York 13790 (personal communication, 1991).
- [11] H.J. Eichler, R. Menzel, R. Sander, and B. Smandek, "Reflectivity Enhancement of Stimulated Brillouin Scattering Liquids by Purification," *Opt. Comm.*, 89, 260-262 (1992).